Modelling of the thermal expansion for high-end 3D printed materials during an autoclave cycle

Master's Thesis

Aharon Baumgarten
Department of Material Science & Engineering

Supervisor company: Reinier Haverkamp Begemann
Supervisor TU: Georgy Filonenko

March 3, 2025

Abstract

This research focuses on modeling the thermal expansion behavior of high-end 3D printed fiber-reinforced polymer composites during autoclave cycles. Utilizing a combination of finite element analysis (FEA), analytical modeling, and experimental thermo-mechanical testing, the study aims to predict and validate the coefficient of thermal expansion (CTE) of these materials.

The investigation primarily examines the influence of fiber orientation and void content on thermal expansion properties. Experimental techniques, including optical microscopy, x-ray tomography, and dynamic mechanical analysis (DMA), were employed to assess microstructural properties and thermal behavior. Results indicate that the use of a breaker plate during extrusion enhances random fiber orientation, promoting isotropic thermal expansion.

The CTE values for aligned and random fiber orientations were analytically modeled using short fiber-reinforced polymer (SFRP) models, demonstrating good alignment with experimental data trends. The study also found that void content only minimally affects CTE, contributing to a slight increase of approximately 5%.

Despite discrepancies between FEA predictions and experimental outcomes, FEA remains a valuable tool for identifying thermal expansion trends and guiding manufacturing process optimizations. Future work should refine modeling assumptions and expand experimental validation to enhance the predictive accuracy of thermal expansion behavior in large-format 3D-printed molds.

Contents

Chapter 1

Introduction

1.1 Background information

In this section some background information is given about the company where the research is done. Also some theory about AM (Additive Manufacturing) and LFAM (Large Format Additive Manufacturing) is given. The research problem is stated with the corresponding research question. Furthermore, scientific and social relevance of the literature review is described. The search strategy used to find the papers and documents was mainly through Google Scholar and the TU Delft Worldcat database. The keywords used to find the papers and documents where based on ”Short Fiber Reinforced Composites”, ”CTE value”, ”CTE value for injection molding”, ”Thermal analysis”, ”Thermal expansion”, ”CTE value for filled polymers” and a combination of these keywords.

1.1.1 Large Format Additive Manufacturing

Additive manufacturing is a process of creating objects by adding material layer by layer, as opposed to traditional manufacturing, which removes material (subtractive). Using 3D design files, machines like 3D printers build up materials such as plastic, metal, or resin to form parts or products. It allows for complex shapes, reduced waste, and is used in industries like aerospace, automotive, and healthcare for rapid prototyping and custom production.

LFAM (Large Format Additive Manufacturing) is a 3D printing technique designed for producing large-format objects, such as tooling or industrial components, by adding material layer by layer. It employs larger nozzles and higher material throughput compared to standard methods. Pellet extrusion, a key feature of LFAM, uses plastic pellets instead of filaments, allowing for faster production and the use of a broader range of materials, including advanced composites like carbon fiber-reinforced polymers. This approach is more cost-effective and supports the creation of robust, large-format parts.

CEAD is a 3D print company that builds large format 3D printers, and also helps with the implementation of large format thermoplastic composite 3D printing solutions. The technical components CEAD offers includes pellet extruders as complete standalone systems, with a base unit that controls the parameters of the extruder. The extruders can process fiber-filled thermoplastic pellets which offer cost-effective and high performance quality.

In addition to extruders, CEAD also offers print beds and complete systems customized to meet the needs of the customer (Figure 1.1).

Figure 1.1: Complete system

1.1.2 Material

In this section the materials used in the research are described. A composite material is a ”mixture” of two substances, creating a new substance. The composite material being used in this research consists out of a polymer filled with fibers. The polymers that are used in 3D printing are mostly thermoplastic (material that can be softened through heating and then processed). The fibers are made out of glass or carbon fibers, but can also include natural fibers like wood. The fibers can align in a certain direction, and can be either continuous or discontinuous throughout the material. Figure 1.2 shows the classification of composites. The classification of the composite used in this research is as followed: composite consisting out of fibers that are discontinuous (short) and either aligned or randomly orientated. Two specific materials will be used in the research. The first one is a fiber filled modified PEI (Polyetherimide) with 20% carbon fiber content. The second material is fiber filled PC (Polycarbonate) with 20% carbon fiber content. The reason why these specific materials are chosen for this research, is that both materials are widely used in the mold making industry, due to their high thermal stability (which will be explained in the next section).

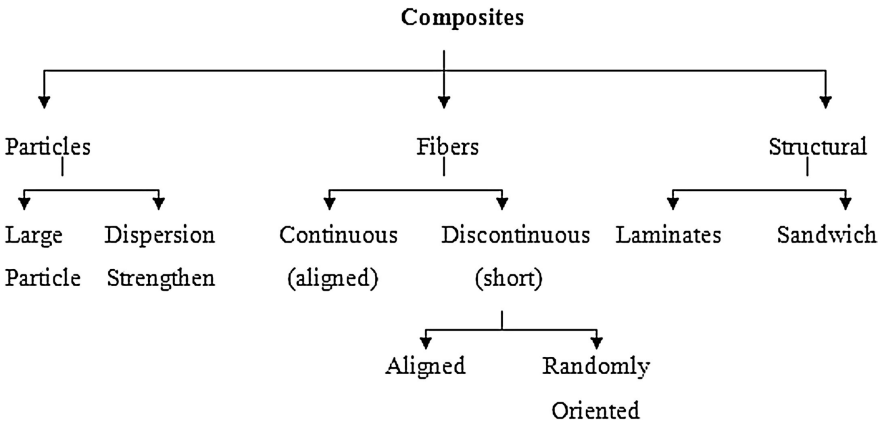

Figure 1.2: Classification of composites [1]

Chemical structure

The PEI used in this project is called Polyetherimide. Polyetherimides are thermoplastics that are known to have an amorphous structure with repeating units of ether and imide (see Figure 1.3). It is not to be confused with Polyethyleneimine, which consists is also a polymer, but consists out of linear or branched ethylene and imine groups.

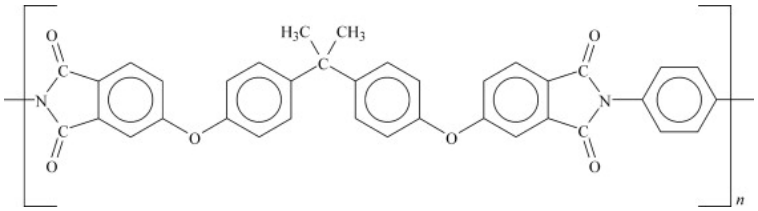

Figure 1.3: Chemical structure of Polyetherimide [2]

Polycarbonate (PC) consists out of repeating units containing carbonate groups. PC is a thermoplastic that is composed out of a long molecular chain, consisting out of rigid molecular chain, depicted in Figure 1.4.

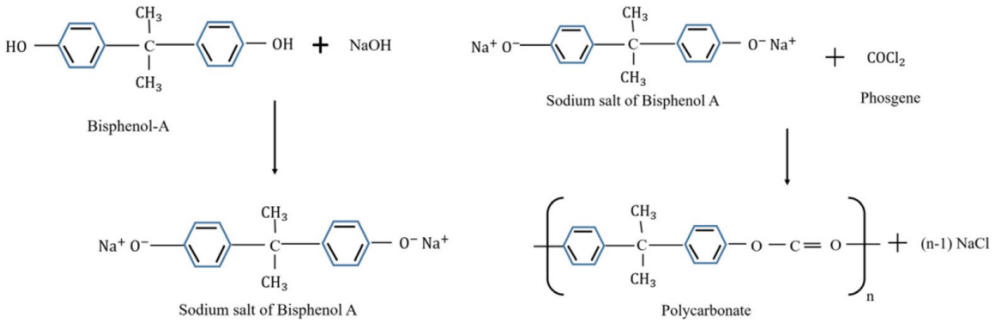

Figure 1.4: Chemical structure of PC [3]

Table 1.1 shows some of the main differences between Polycarbonate (PC) and Polyetherimide (PEI). However, it is noted that both of these materials have a (relatively) high thermal stability.

Property	**Polycarbonate (PC)**	**Polyetherimide (PEI)**
Chemical structure	carbonate groups	Ether and imide groups
Thermal stability	Moderate thermal stability (up to $\approx 120^{\circ}$C)	High thermal stability (up to $\approx$ 180 – 200°C)
Mechanical strength	High impact resistance and toughness	High tensile strength and rigidity
Chemical resistance	Moderate resistance to chemicals	Excellent resistance to chemicals and acids
Cost	Relatively low	Higher due to specialized applications

Table 1.1: Properties of PC and PEI

Mechanical- and Thermal properties

Both of the materials have been tested on mechanical- and thermal properties, by the manufacturer of the material. The mechanical properties are summarized in Table 1.2. The X is the bead print direction and Z is through the bead thickness.

Properties	**Modified PEI with 20% carbon fiber**	**Modified PC with 20% carbon fiber**
Tensile strength X	126 MPa	112.4 MPa
Tensile strength Z	68 MPa	50.3 MPa
Tensile modulus X	11.7 GPa	11 GPa
Tensile modulus Z	3.8 GPa	3 GPa
Elongation at break X	1.3%	1.5%
Elongation at break Z	2.3%	1.8%
Flexural strength X	194 MPa	180 MPa
Flexural strength Z	107 MPa	93.8 MPa
Flexural modulus X	13.1 GPa	10.8 GPa
Flexural modulus Z	4.1 GPa	3.8 GPa
Shear strength XZ	53 MPa	38.6 MPa
Shear strength ZX	48.3 MPa	39 MPa
Shear modulus XZ	1.28 GPa	1.1 GPa
Shear modulus ZX	1.45 GPa	1.23 GPa
Compressive strength X	186.3 MPa	141 MPa
Compressive strength Z	146.6 MPa	113.7 MPa
Poisson's ratio ν_{13}	0.319	0.32
Poisson's ratio ν_{31}	0.108	0.115
Density as printed	1.15 g/cc	1.21 g/cc

Table 1.2: Mechanical properties for PEI and PC reinforced with carbon fiber [4]

The thermal properties are summarized in Table 1.3. The coefficient of thermal expansion is already determined for both of the materials using a standard test by the manufacturer of the material (ASTM E831, more described in Section 2.1.3).

Properties	**Modified PEI with 20% carbon fiber**	**Modified PC with 20% carbon fiber**
T_g (onset)	221°C	154 °C
T_g (Tan Delta)	236 °C	163 °C
Coefficient of thermal expansion X	7.58 ppm/°C	10.88 ppm/°C
Coefficient of thermal expansion Z	74.87 ppm/°C	110.07 ppm/°C
Specific Heat	1.683 J/(g°C)	1.657 J/(g°C)
Thermal conductivity X	1.18 W/(m°K)	1.07 W/(m°K)
Thermal conductivity Z	0.28 W/(m°K)	0.32 W/(m°K)

Table 1.3: Thermal properties for PEI and PC reinforced with carbon fiber [4]

Processing parameters

In this section some information is given about the processing parameters of the material. The material being researched for this application is specifically used for making molds. On these molds, prepregs (mats filled with fibers in a specific direction and resin) are deposited on the mold surface to be cured and hardened. This curing/hardening of the prepreg usually requires a vacuum seal and a temperature cycle. This is done by putting the product (mold with prepreg) in an autoclave. The autoclave is an oven that is also pressurized (see Figure 1.5). So not only is the prepreg under pressure (vaccuum), but the whole mold is also under pressure. To gain the maximum dimensional accuracy for the product, it is important that the mold also remains dimensionally stable during the autoclave cycle (as much as possible). This directly relates to the coefficient of thermal expansion (CTE) of the material, which relates the temperature change to the dimension change.

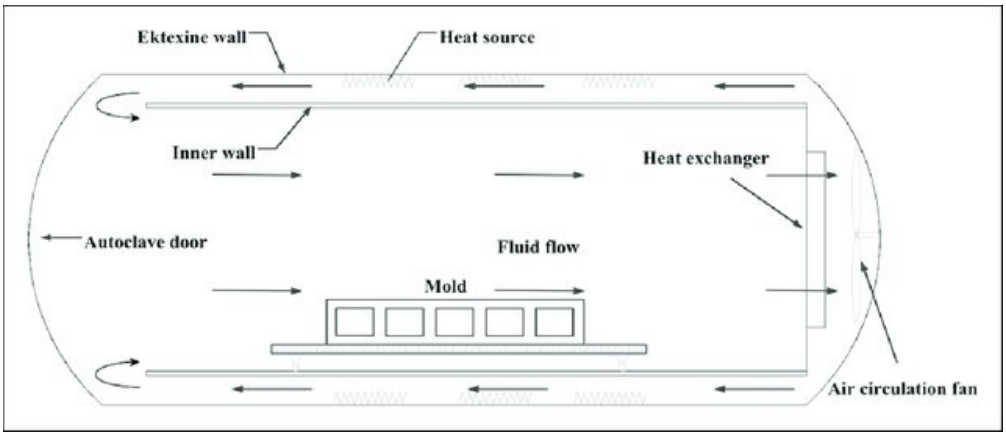

Figure 1.5: A typical autoclave system [5]

Examples of autoclave cycles for the materials used in this research are shown in Figures 1.6 and 1.7. The cycles depend on the type of composite being deposited on the mold. The cycles shown here are based on a typical composite used for aerospace and automotive applications. The graphs show the temperature and pressure change as a function of the time. For the temperature, a ramp up and cooling rate of 0.5-1.5°C/min is typically used, and for the pressure a rate of 0.14-0.34 bar/min is typically used.

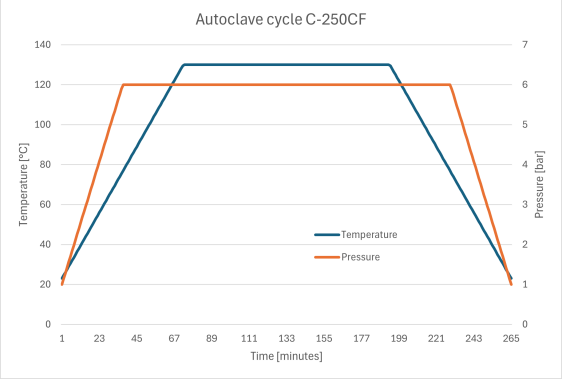

Figure 1.6: Autoclave cycle for PC 20% fiber

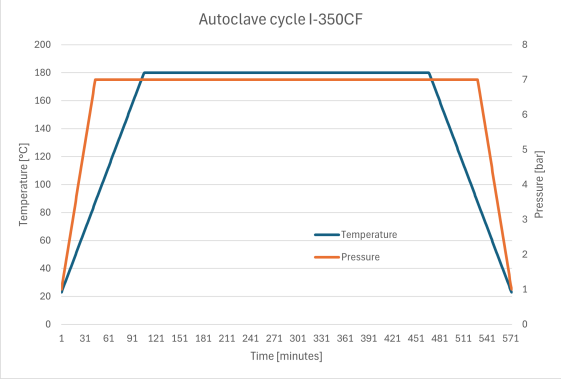

Figure 1.7: Autoclave cycle for PEI 20% fiber

The processing parameters for both of the materials are shown in Table 1.4 as given by the manufacturer of the material. The material is dried before use, to minimize the moisture and void content of the material during printing.

Properties	**Modified PEI with 20% carbon fiber**	**Modified PC with 20% carbon fiber**
Drying Maximum moisture content	0.02 %	0.02 %
Extruder zone 1 Temp	332°C	227°C
Extruder nozzle Temp	410°C	338°C

Table 1.4: Processing parameters for PEI and PC reinforced with carbon fiber [4]

The autoclave cycle (shown in Figures 1.6 and 1.7) consists out of a few steps. Below a typical autoclave cycle is described for a mold. For this research, the bagging and unbagging of the prepreg, and any other additional steps of the prepreg will not be taken into account. The interest lies with the pressure and temperature build up, holding and cooling down of the mold itself.

1. Temperature and pressure build-up. Here the temperature and pressure are gradually increased to a specific ramp-up schedule, depending on the composite.
2. Holding of the temperature and pressure for a specific time.
3. Cooling of the material. Also done with a specific rate so that the material does not warp or deform too much.

1.1.3 Single Screw Extruder

This section explains how the material is printed, and how one of the main components of a CEAD printer works. Figure 1.8 schematically shows how the material (in the form of pellets) enters an extruder, and how it is deposited on the printbed. Before entering the hopper (as shown in the figure) the pellets are first dried in a dryer, to remove most of the moisture. From the dryer, the pellets are fed through a hopper, where from there the pellets enter the beginning of the screw. The screw is driven by a electric stepper motor and the pellets are moved down to the nozzle. The pellets pass through four heating zones (five when using a melt pump).

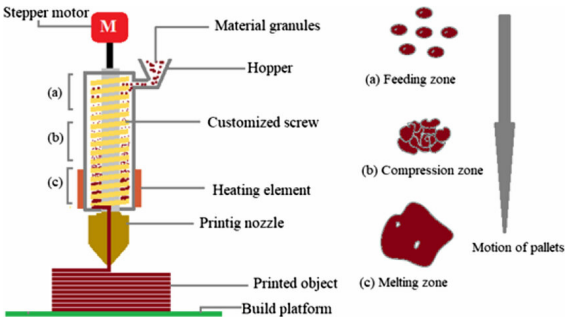

Figure 1.8: Pellet extruder schematics [6]

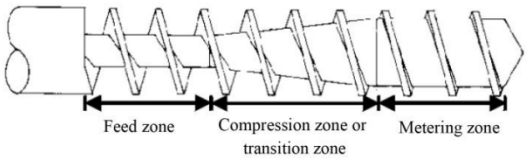

Figure 1.9: Zones in a single-screw extruder [7]

Figure 1.9 shows the different geometrical zones in a typical single-screw extruder. The first zone is the feed zone. The feed zone has a constant channel depth. This is where the material is still in a solid state. The second stage is the compression zone. Here the channel depth progressively gets shallower. The material gets converted from the solid state to the molten state (coexistence of solid and molten material). The third stage is the metering zone, where the entire polymer is molten and where the channel depth is again constant [7].

Some optional components of the extruder are a breaker plate and a melt pump (or Dynamic Flow control). The DFC module (Dynamic Flow Control) is placed between the last heating zone and the nozzle. The function of the DFC module is to control the output of the material. This principle is illustrated in Figure 1.10. The melted material passes through two interlocking gears, and the output can be controlled by changing the speed of the gears.

The breaker plate is a round metal plate with holes in it, usually placed in the nozzle. Figure 1.11 shows an example of a breaker plate, containing 9 holes all with a diameter of 3 mm. The breaker plate is typically selected with a 1:1.5 ratio of breaker plate holes to nozzle area (based on research performed by CEAD). The functions of the breaker plate include the conversion from spiral flow of melt into stream lined laminar flow. Also the breaker plate holds back any contamination and un-melted particles [8].

Both the DFC module and breaker plate are expected to have an influence on the fiber orientation of the composite during the deposition on the print bed. It will be interesting to see the difference in fiber orientation between these components, and how this will effect the thermal expansion of the material.

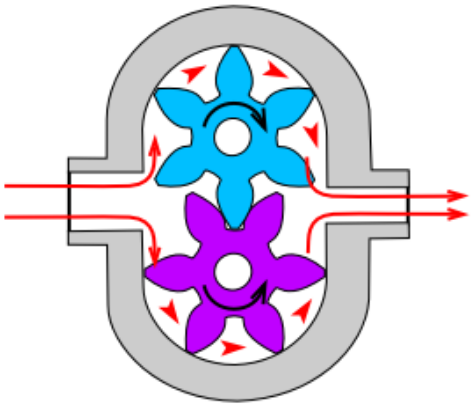

Figure 1.10: Working principle melt pump

Figure 1.11: 9x3 mm breaker plate

The geometry terminology of the printed object is schematically shown in Figure 1.12. This terminology will be further used in the research. The area marked by red is referred as a single bead. Layer width in 3D printing refers to the width of each extruded line, which affects strength and finish, whereas layer height is the thickness of each layer, which affects smoothness and print time. The interior structure is described by infill. A higher infill offers greater strength but takes longer.

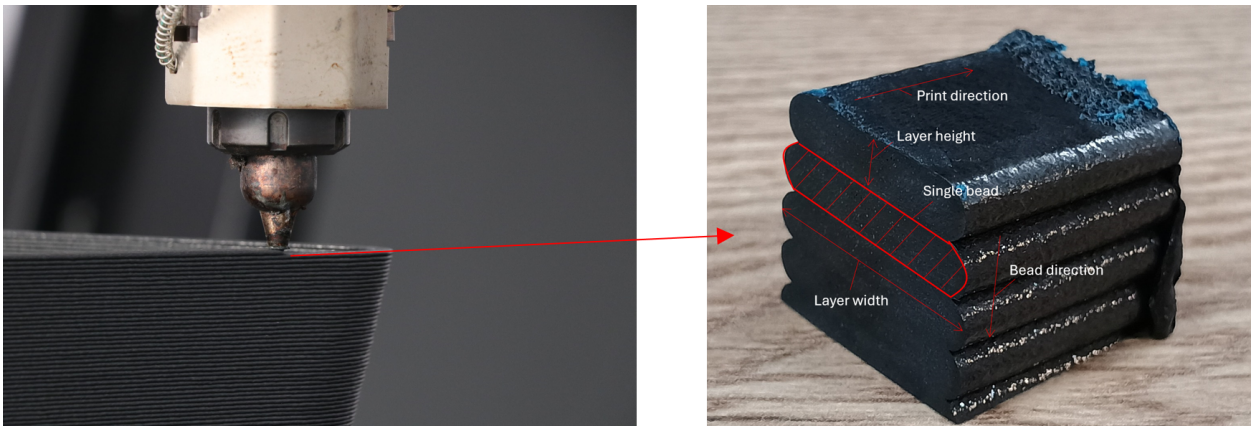

Figure 1.12: Geometry of 3D printed object

1.2 Research problem

The Coefficient of Thermal Expansion (CTE) value is directly related to the expansion or shrinkage of the material when exposed to a temperature change. For making molds it is important that the expansion of the product is minimal (or at least known) when exposed to a heating cycle.

For 3D printing materials, pellets made out of a thermoplastic polymer are used with a certain amount of short fibers. These pellets are melted and deposited onto the print bed, giving the fibers a specific orientation. The carbon fibers have a lower CTE value then the surrounding matrix, and therefore are expected to influence the CTE value of the whole composite, depending on the orientation and other material contaminations (like voids). Some CTE measurements have been performed (using TMA) by clients, and the expected results do not match the results from the measurements.

The goal is to get more insight into the thermal expansion of fiber-filled polymers for high-end (high temperature) 3D printed products during an autoclave cycle, by including the specific fiber properties and material contaminations. Below the research question is stated in one sentence:

Modelling of the thermal expansion for high-end 3D materials during an autoclave cycle

1.2.1 Scientific- and Social relevance

The research being done on the thermal expansion for high-end 3D printed materials have both scientific and social relevance. Scientifically, the research contributes to the knowledge on how fiber-filled polymer composites react under fluctuating temperature and pressure, which is crucial for optimizing parts made by LFAM. The result of this research will hopefully give more insight on how the fiber properties (orientation, size of the fibers, etc.) and contaminations (voids) will influence the thermal expansion of the material. Based on these results, a recommendation is made on what kind of material is ideal for this specific application.

Socially, this research is relevant for all kinds of industries like aerospace, automotive and many more. The materials used in this research are particularly being used for molds, where composite prepregs are laid upon, and cured in an autoclave. Knowing precisely how the material will expand in an autoclave, before being printed will enhance the efficiency of the process and improve the accuracy of the product.

Chapter 2

Thermal Expansion

In this chapter the theory behind the thermal expansion is explained, using papers and useful resources. Also how the thermal expansion applies to the high-end 3D printed composite materials used in CEAD. Furthermore, some testing methods are stated that can be used to determine the thermal expansion of a composite material.

2.1 Theory

The tendency of a material to expand in volume as temperature rises is known as thermal expansion. Thermal expansion is caused by atoms that vibrate due to an increase in the temperature (internal energy), and as a result of the vibration, the distance between the molecules also increase (expansion). Usually, the fractional change in length or volume per degree of temperature change is used to quantify it. A volumetric linear expansion coefficient (Equation 2.1) is typically used to characterize this for solids (in accordance with the standard test procedure for linear thermal expansion of solid materials by thermal mechanical analysis). When it comes to isotropic crystalline solids, the expansion happens uniformly in every direction due to their uniform structure. Equation 2.2 indicates that as the temperature changes, a change in shape may result from differing expansion rates along distinct crystallographic directions if the crystal structure is not isotropic [9]. For the 3D printed materials mentioned in section 1.1.2, this is the case.

$$\alpha = \frac{1}{V}\left(\frac{\partial V}{\partial T}\right)_p \tag{2.1}$$

$$\alpha_x = \frac{1}{L_x}\frac{dL_x}{dT}; \alpha_y = \frac{1}{L_y}\frac{dL_y}{dT}; \alpha_z = \frac{1}{L_z}\frac{dL_z}{dT} \tag{2.2}$$

In Equation 2.1, α stands for the coefficient of linear thermal expansion, and α_x, α_y and α_z are the coefficients of thermal expansion in the three directions. The change of lengths is given by dL_x, dL_y and dL_z, while the change of temperature is given by dT. The subscript p stand for a constant pressure during the temperature change.

The interest lies with knowing what the thermal expansion is as a function of both temperature and pressure, over a time period (so of the form $\partial T/\partial t$, and $\partial p/\partial t$).

Equation 2.1 has as variables the temperature and volume change. These variables have to be determined by testing the material. Ideally some analytical model would be preferred that can predict the thermal expansion of the material, without thermal mechanical testing. For this some analytical models are presented that can be used to determine the CTE value of short fiber composites, and how to create a model that can predict the expansion. Eventually, the result should be of the form where the volume change is related to both the thermal expansion caused by the temperature change and compression as a function of time, as shown in Equation 2.3.

$$\Delta V = V_0 \alpha T(t) + V_0 \varepsilon P(t) \tag{2.3}$$

2.1.1 Analytical models

This section covers some analytical models that can be used to determine the CTE value for composites with (partially) aligned distributed particles. There are more analytical models available on determining the CTE values of composites, however, the review has been reduced to only including analytical models specifically for short fiber composites. Also the widely known "Rule of Mixtures" has been left out, since it is a too simple formulation, and does not include the fiber properties and orientation.

M-T model

The Mori-Tanaka model estimates the effective properties of the composite by means of a mean-field homogenisation technique. It is assumed that the inclusions (fibers) are contained within an infinite matrix and that an average field technique is used to account for the interaction between the inclusions [10]. The geometry of the inclusion is defined as fiber-liked particles ($a_1 > a_2 = a_3$) as shown in Figure 2.1.

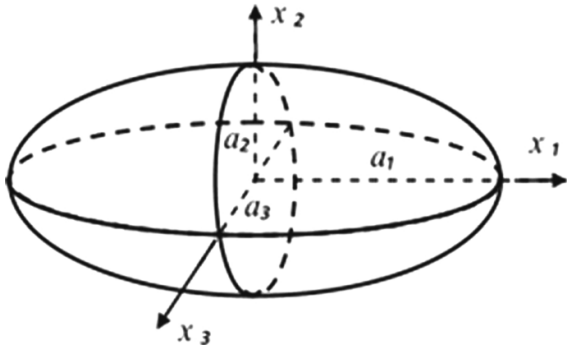

Figure 2.1: Geometry and coordinate system of an inclusion [10]

The prediction for the CTE values in the alignment direction (α_{11}) and along the transversal directions ($\alpha_{22} = \alpha_{33}$) are given by the relations shown in Equations 2.4 and 2.5, where α_m and α_f represent the linear thermal expansion coefficients of the matrix and the filler. f_p is the volume fraction of the particles. The expressions for E_i and B are given in the paper [10] and are related to the geometry, alignment, mechanical properties and aspect ratio of the particles.

$$\alpha_{11} = \alpha_m + f_p \frac{(2E_2 - E_4 - E_5)}{2E_2E_3 - E_1(E_4 + E_5)} B(\alpha_f - \alpha_m) \tag{2.4}$$

$$\alpha_{22} = \alpha_{33} = \alpha_m + f_p \frac{E_3 - E_1}{2E_2E_3 - E_1(E_4 + E_5)} B(\alpha_f - \alpha_m) \tag{2.5}$$

SFRP composites

[11] describes the thermal expansion of short fiber reinforced polymer composites (SFRP). These equations take into account the properties of the short fibers. The CTE values parallel to the fibers (1-direction) and transverse to the fibers (2-direction) are given in Equations 2.6 and 2.7.

$$\alpha_1^0 = \frac{\lambda E_f \alpha_f \nu + E_m \alpha_m (1-\nu)}{\lambda E_f \nu + E_m (1-\nu)} \tag{2.6}$$

$$\alpha_2^0 = (1+\nu_f)\alpha_f \nu + (1+\nu_m)\alpha_m \nu_m - \alpha_1^0 \nu_{12} \tag{2.7}$$

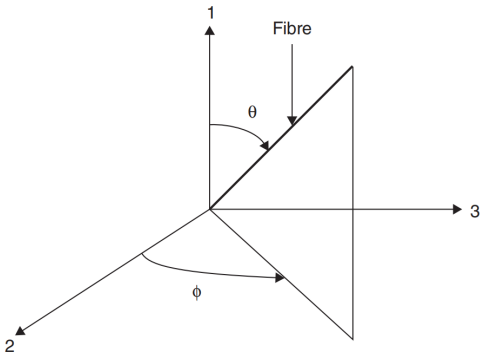

Figure 2.2: Angle θ that the fiber has with the 1 direction [11]

λ includes the properties of the short fibers, and are further described in the paper [11]. Depending on the orientation of the fibers the value of the CTE in both directions change. Figure 2.2 shows the angle θ that the fiber has with the 1-direction. Equations 2.8 and 2.9 include the fiber orientation in the composite.

$$\alpha_1 = \alpha_1^0 \cos^2\theta + \alpha_2^0 \sin^2\theta \tag{2.8}$$

$$\alpha_2 = \alpha_1^0 \sin^2\theta + \alpha_2^0 \cos^2\theta \tag{2.9}$$

Compression due to pressure

During the autoclave process, not only is there a temperature cycle, but there is also a pressure cycle. The pressure in an autoclave is used to minimize the voids in the prepreg, by compressing the resin in the composite, and evenly distributing the resin over the surface of the mold. For determining the total expansion during an autoclave cycle, it is therefore important to take the compression into account.

For unidirectional short fiber composites, the longitudinal elastic modulus can be obtained using the Cox shear lag model [11] (shown in Equation 2.10). Again here, λ includes the properties of the fibers (alignment, geometry, mechanical properties).

$$E_c = \lambda E_f \nu + E_m (1-\nu) \tag{2.10}$$

The transverse modulus and in-plane shear modulus are nearly independent of the fiber orientation and can be determined using the Halpin-Tsai equations (shown in the paper [11]). Using the components of the stiffness matrix, the strain can be related to the stress through a compliance matrix (Equation 2.11).

$$\begin{bmatrix} \varepsilon_1 \\ \varepsilon_2 \\ \varepsilon_3 \\ \gamma_{23} \\ \gamma_{13} \\ \gamma_{12} \end{bmatrix} = \begin{bmatrix} S_{11} & S_{12} & S_{13} & 0 & 0 & 0 \\ S_{12} & S_{22} & S_{23} & 0 & 0 & 0 \\ S_{13} & S_{23} & S_{33} & 0 & 0 & 0 \\ 0 & 0 & 0 & S_{44} & 0 & 0 \\ 0 & 0 & 0 & 0 & S_{55} & 0 \\ 0 & 0 & 0 & 0 & 0 & S_{66} \end{bmatrix} \cdot \begin{bmatrix} -P \\ -P \\ -P \\ 0 \\ 0 \\ 0 \end{bmatrix} \tag{2.11}$$

This relation can be used to determine the strain in the principle directions. In Equation 2.11, P is the applied pressure in the autoclave (negative because it is compression). The compliance matrix components can be determined using the elastic modulus components, shown in the paper [11].

2.1.2 Finite Element Analysis

A way for predicting the thermal expansion of a three-phase composite consisting out of discontinuous aligned fibers is Finite Element Analysis (FEA). In this section, the basics behind FEA is briefly explained and how a typical three-phase composite could be modelled for FEA use. FEA is a numerical method used to solve partial differential equations, by discretization of the model into smaller and simpler parts called finite elements.

For characterizing the geometry for the use in FEA, the composite (discontinuous fiber reinforces) can be either modelled as the whole model (field homogenization) or as a Representative Volume Element (RVE). A RVE model directly models the fibers and matrix without any simplification and can be used to determine the properties of a material on a microscale . Figure 2.3 shows an example of a RVE model for a 3D printed composite material.

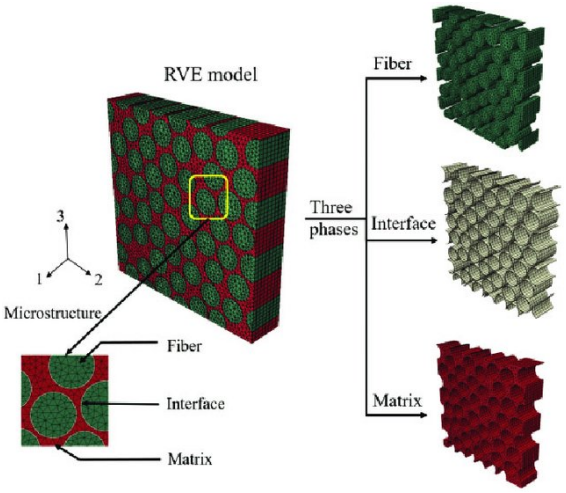

Figure 2.3: RVE model setup example [12]

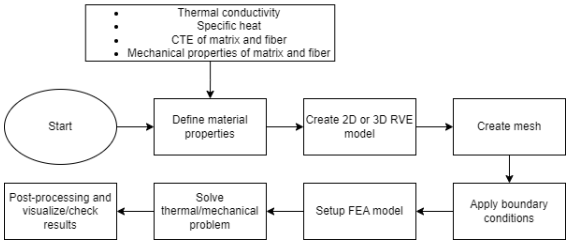

Figure 2.4: Flowchart steps for FEA

Figure 2.4 shows the steps required to create a FEA model using either a 2D or 3D RVE model. For defining the material properties of the fiber and matrix, the M-T model or equation for SFRP can be used. The downside to using a RVE model is that it results in a complex geometry which in turn requires high computational requirements. Using field homogenization, the properties of the material are homogenized across the model. By including the fiber orientation in the material properties, it is also expected that this technique will be sufficient for determining the thermal expansion, without the need for complex geometries.

The type of meshes/element that are typically used in FEA are shown in Figure 2.5.

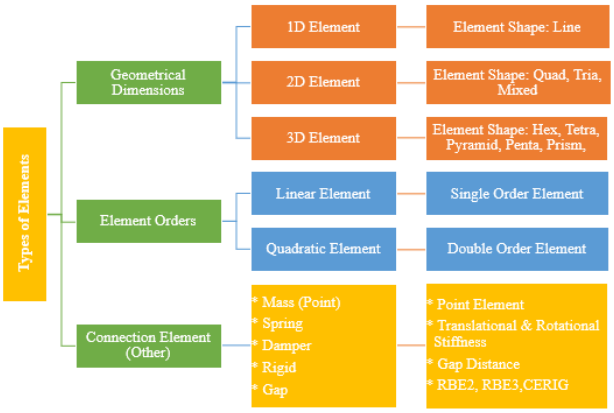

Figure 2.5: Types of FEA elements [13]

The type of element that is used depends on the geometry and the type of analysis that has to be performed. Based on how the model looks, 2D or 3D elements can be used for the calculation. The thermomechanical problem that has to be solved is the expansion (reaction) of a model under a temperature and pressure change. These are two problems that have to be solved. One mechanical (compression caused by pressure change) and one thermal (expansion caused by temperature change).

The thermomechanical problem that can be solved using FEA is the heat equation (Equation 2.12). In this equation α is the thermal diffusivity of the material, not the thermal expansion coefficient. This equation will give the temperature distribution within the material over time.

$$\frac{\partial T}{\partial t} = \alpha \left(\frac{\partial^2 T}{\partial x^2} + \frac{\partial^2 T}{\partial y^2} + \frac{\partial^2 T}{\partial z^2} \right) \tag{2.12}$$

$$\alpha = \frac{k}{\rho c_p} \tag{2.13}$$

In Equation 2.13, the k is the thermal conductivity, ρ is the density and c_p is the specific heat capacity. For short fiber composites, the thermal conductivity is (similar to the CTE value) different in different directions due to the anisotropic nature of the material. Equation 2.12 actually becomes Equation 2.14.

$$\rho c_p \frac{\partial T}{\partial t} = \frac{\partial}{\partial x}\left(k_x \frac{\partial T}{\partial x} \right) + \frac{\partial}{\partial y}\left(k_y \frac{\partial T}{\partial y} \right) + \frac{\partial}{\partial z}\left(k_z \frac{\partial T}{\partial z} \right) \tag{2.14}$$

When the material is heated, the temperature increases according to the heat equation. This temperature distribution (T(x,y,z,t)) can be used to calculate the local temperature change (ΔT) at any point in the material (model). Using the local temperature change, the thermal expansion can then determine the change in dimensions of the material at different points.

FEA does not solve the original differential equation (Equation 2.14), but makes an approximation of the ”weak form” of the heat equation [14]. The reason for this is to make the equation more easy to solve numerically.

To obtain the weak formulation of the "strong" form of the heat equation, the equation is first multiplied with a test function v, and integrated over the volume Ω (Equation 2.15).

$$\int_{\Omega} \rho c_p \frac{\partial T}{\partial t} v d\Omega = \int_{\Omega} v \left[\frac{\partial}{\partial x}\left(k_x \frac{\partial T}{\partial x}\right) + \frac{\partial}{\partial y}\left(k_y \frac{\partial T}{\partial y}\right) + \frac{\partial}{\partial z}\left(k_z \frac{\partial T}{\partial z}\right)\right] d\Omega \tag{2.15}$$

The next step is to integrate the obtained function by parts (divergence theorem). This will reduce the order of derivatives. For the x component of the formula, the term becomes as shown in Equation 2.16. The same is done for the y and z components of the equation. Here Γ_x represents the boundary of the domain in the x direction, and n_x the component of the normal vector outward on the boundary.

$$\int_{\Omega} v \frac{\partial}{\partial x}\left(k_x \frac{\partial T}{\partial x}\right) d\Omega = -\int_{\Omega} \frac{\partial v}{\partial x} k_x \frac{\partial T}{\partial x} d\Omega + \int_{\Gamma_x} v k_x \frac{\partial T}{\partial x} n_x d\Gamma \tag{2.16}$$

The next step is to combine the terms (Equation 2.15 with Equation 2.16), to obtain the final weak form of the equation.

$$\int_{\Omega} v \rho c_p \frac{\partial T}{\partial t} d\Omega = -\int_{\Omega} \left(k_x \frac{\partial T}{\partial x}\frac{\partial v}{\partial x} + k_y \frac{\partial T}{\partial y}\frac{\partial v}{\partial y} + k_z \frac{\partial T}{\partial z}\frac{\partial v}{\partial z}\right) d\Omega + \int_{\Gamma} v \left(k_x \frac{\partial T}{\partial x} n_x + k_y \frac{\partial T}{\partial y} n_y + k_z \frac{\partial T}{\partial z} n_z\right) d\Gamma$$

In the above Equation the $\int_{\Gamma}$ represents the natural boundary conditions. The final weak form is shown in the Equation below.

$$\int_{\Omega} v \rho c_p \frac{\partial T}{\partial t} d\Omega + \int_{\Omega} \left(k_x \frac{\partial T}{\partial x}\frac{\partial v}{\partial x} + k_y \frac{\partial T}{\partial y}\frac{\partial v}{\partial y} + k_z \frac{\partial T}{\partial z}\frac{\partial v}{\partial z}\right) d\Omega = \int_{\Gamma} v \left(k_x \frac{\partial T}{\partial x} n_x + k_y \frac{\partial T}{\partial y} n_y + k_z \frac{\partial T}{\partial z} n_z\right) d\Gamma$$

To use this for finite element calculation use, shape functions ($N_i(x, y, z)$ are chosen for each node of the finite elements. These shape functions approximate the temperature in each element. In Equation 2.17, T_i represents the temperature at node i and n is the total number of nodes in the element.

$$T(x, y, z) = \sum_{i=1}^{n} N_i(x, y, z) T_i \tag{2.17}$$

The shape function can be substituted in the final form of the weak function, assuming the test function is equal to the shape function, and a global system of equations can be obtained (Equation 2.18).

$$M\frac{dT}{dt} + KT = F \tag{2.18}$$

In Equation 2.18, M is the mass matrix, K is the stiffness matrix and F is the force vector, defined as below. It is expected that these equations can be used for FEA calculations of the thermomechanical problem.

$$M_e = \int_{V_e} \rho c_p N_i N_j dV$$

$$K_e = \int_{V_e} \left(k_x \frac{\partial T}{\partial x}\frac{\partial v}{\partial x} + k_y \frac{\partial T}{\partial y}\frac{\partial v}{\partial y} + k_z \frac{\partial T}{\partial z}\frac{\partial v}{\partial z}\right) dV$$

$$F_e = \int_{\Gamma_e} N_j \left(k_x \frac{\partial T}{\partial x} n_x + k_y \frac{\partial T}{\partial y} n_y + k_z \frac{\partial T}{\partial z} n_z\right) d\Gamma$$

2.1.3 Test methods

There are several techniques available on the market for testing the CTE value of a material. Testing the CTE value will be necessary for validating the analytical model. Some of these testing methods are described in this section. Depending on what is available at the department of Material Science & Engineering, one of these methods will be used to determine the thermal expansion.

Thermomechanical Analysis (TMA)

Thermomechanical analysis measures the deformation of a material when subjected to a temperature change. This is done by subjecting the sample under a nonoscillatory load and measuring the changes in the sample dimensions as a function of temperature and time [15]. Figure 2.6 shows a schematic diagram of a typical TMA instrument. This device is also used as standard test method for solid material (ASTM E831-19).

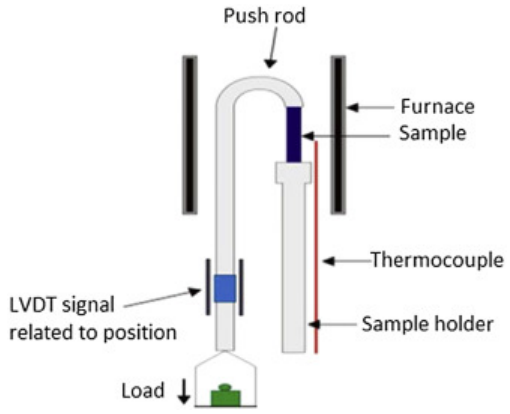

Figure 2.6: Schematic diagram of a typical TMA analyzer [15]

Dilatometry

Dilatometry measures the same as a thermomechanical analysis, except that for dilatometry there is no applied load. It is a technique where a sample is heated in a chamber and changes in the dimensions is measured by an extensometer. The change in length to its original length enables the thermal strain to be determined over a specific temperature range, and this can be used to determine the CTE value of the material [16].

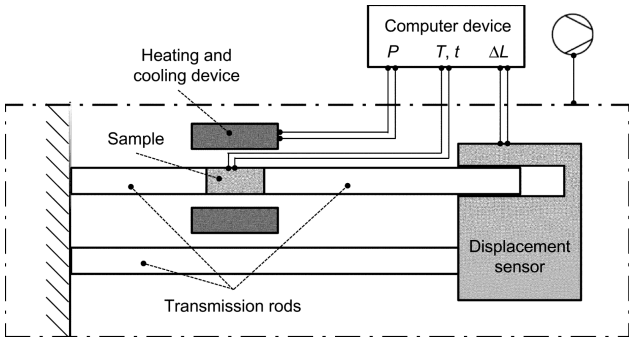

Figure 2.7: Schematic diagram of a typical dilatometer [17]

Dynamic Mechanical Analysis (DMA)

Dynamic Mechanical Analysis (DMA) is a technique used to measure the properties of a material by subjecting the sample under periodic stress, and measuring the deformation. In the case of measuring thermal expansion, instead of a periodic stress, a (low) constant load is applied, just enough so that the sample is fixed in between the loading plates. Also, the pressure in an autoclave can be tested by applying a force on the sample corresponding to the applied pressure in the autoclave. The basic working principle of a typical DMA machine is shown in Figure 2.8.

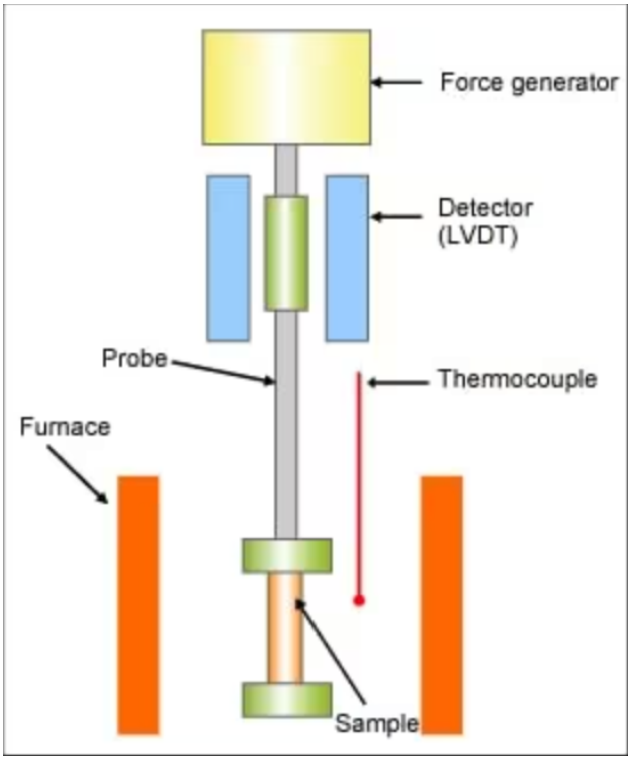

Figure 2.8: Working principle of a DMA [18]

Chapter 3

Results

3.1 Micro-structural properties

The fiber orientation, density and contamination (like air bubbles or foreign material) are expected to have an influence on the determination of the thermal expansion. For this reason, optical microscopy and x-ray tomography have been performed on several samples, and the effect of the melt pump and breaker plate on the micro structure has been investigated. The dimensions of the bead are 21 x 4 mm (layer width x layer height, see Figure 1.12) using a 12 mm nozzle with a 9x3 mm breaker plate. The reason for the specific bead dimension is that a large bead width is typically used for making molds, since the molds need to be relatively large and structurally strong. The 9x3 mm breaker plate consists out of a circular steel plate, placed at the beginning of the nozzle, and it contains 9 holes with each a diameter of 3 mm. This section covers the results of the measurement of the void content and fiber orientation using optical microscopy and x-ray tomography.

3.1.1 Optical Microscopy

Void content

The figures shown below are an example on how the void content was determined. The material shown below is PEI with 20% carbon fiber, with the use of a breaker plate (as described in Section 1.1.2).

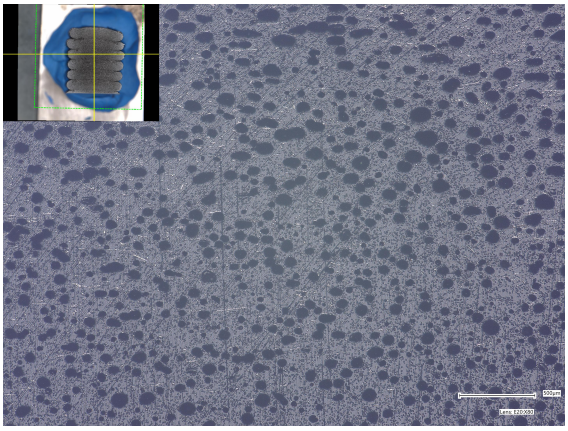

Figure 3.1: PEI void content before (OM 80x)

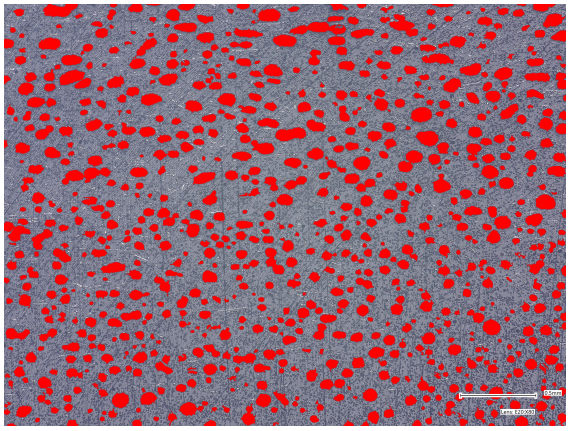

Figure 3.2: PEI void content after (OM 80x)

The optical microscope used in this research is the "VHX 7000 N Digital Microscope" at the department of Material Science & Engineering at the TU Delft. Figures 3.1 and 3.2 show images of the samples cut in the bead direction, and shows the cross section of the samples. The black areas represent the voids in the material. Using OM the void properties (like area content, void diameter, etc.) at multiple locations on the surface of the bead where inspected. This has been done for both materials (PEI and PC) with combinations of different components (breaker plate and DFC module).

In Table 3.1 and Table 3.2 the differences in void properties between the different samples and components are shown for PC and PEI. The data was acquired by taking six images on the surface of one sample and averaging the void properties between these six samples. The void properties where determined in a similar way as shown in Figure 3.2. This information can be used for modeling the structure of the samples in a later stage.

Sample	No breaker plate, no DFC	Breaker plate, no DFC	No breaker plate, DFC	Breaker plate, DFC
Void count	416 ± 96	401 ± 53	206 ± 69	739 ± 190
Void area content	$7.6\% \pm 1.2$	$6.0\% \pm 0.55$	$5.6\% \pm 1.6$	$6.7\% \pm 2.01$
Min average void diameter	$0.15\text{mm} \pm 0.02$	$0.13\text{mm} \pm 0.02$	$0.15\text{mm} \pm 0.01$	$0.12\text{mm} \pm 0.06$
Max average void diameter	$0.22\text{mm} \pm 0.05$	$0.19\text{mm} \pm 0.02$	$0.35\text{mm} \pm 0.16$	$0.30\text{mm} \pm 0.18$

Table 3.1: Differences between samples PC

Sample	No breaker plate, no DFC	Breaker plate, no DFC	No breaker plate, DFC	Breaker plate, DFC
Void count	696 ± 39	792 ± 54	305 ± 46	415 ± 107
Void area content	$16.2\% \pm 0.93$	$22.8\% \pm 1.65$	$15.8\% \pm 1.8$	$12.1\% \pm 3.7$
Min average void diameter	$0.15\text{mm} \pm 0.02$	$0.19\text{mm} \pm 0.05$	$0.19\text{mm} \pm 0.05$	$0.2\text{mm} \pm 0.08$
Max average void diameter	$0.22\text{mm} \pm 0.02$	$0.68\text{mm} \pm 0.47$	$0.44\text{mm} \pm 0.16$	$0.39\text{mm} \pm 0.16$

Table 3.2: Differences between samples PEI

Figures 3.3, 3.4 and 3.5 summarize the results from 3.1 and Table 3.2. From the figures it can be seen that the void content is relatively lower when using a breaker plate or DFC. However, it seems that the standard deviation of the samples are relatively too high to make a conclusion on the void content between the samples. It is expected that the standard deviation is higher due to the higher differences in void sizes. To validate these results, x-ray tomography is performed on two samples, and the results gained from x-ray tomography will be compared to the optical microscope results.

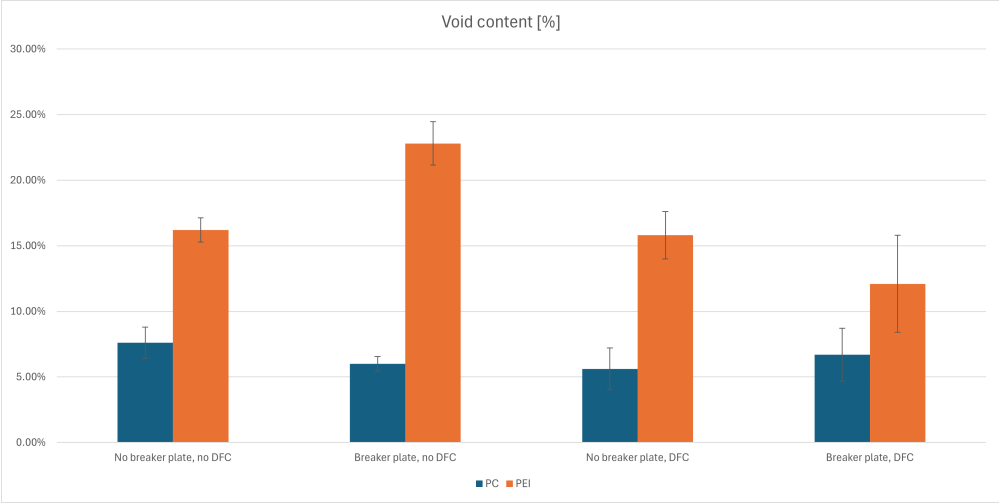

Figure 3.3: Void content PC and PEI

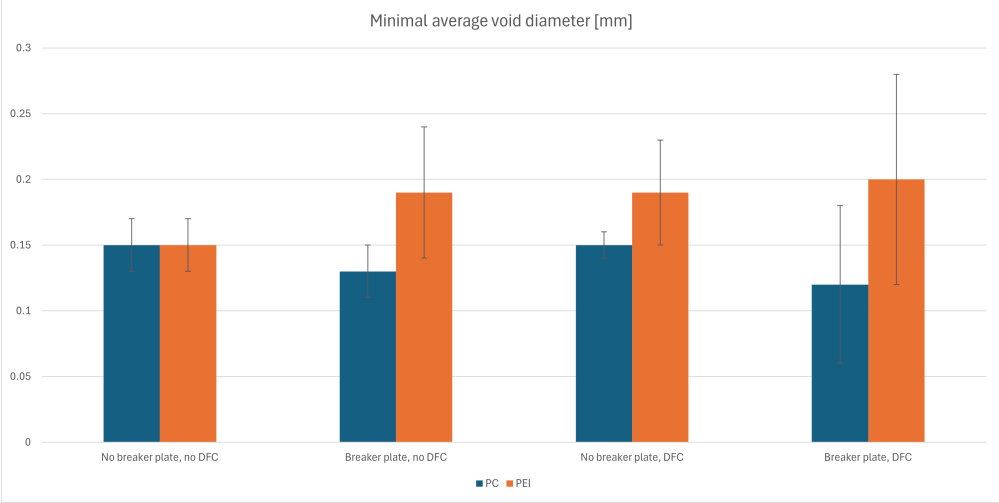

Figure 3.4: Minimal void diameter PC and PEI

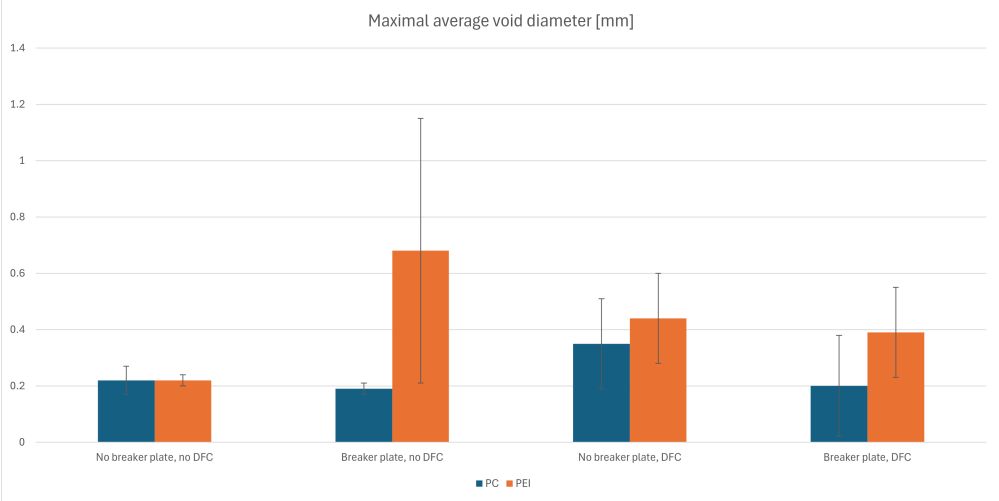

Figure 3.5: Maximum void diameter PC and PEI

Fiber orientation

The material being printed has a specific fiber orientation. It is expected that the fibers rearrange themselves during the deposition of the material onto the printbed. It is therefore important to understand in what way the fibers can orientate themselves, and what this means for the determination of the coefficient of thermal expansion.

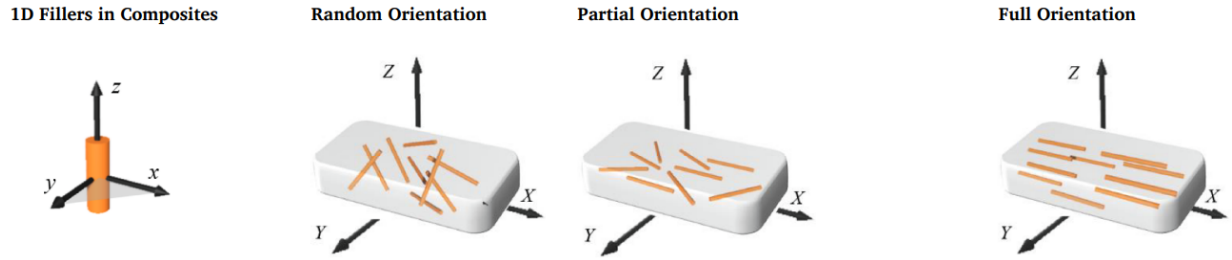

Figure 3.6: Orientation of fillers in composites [19]

Figure 3.6 shows in what ways the fibers/filler can be orientated in the matrix. Figures 3.7 and 3.8 show images of the samples cut in the print direction, and shows the cross section of the samples when not using a breaker plate and when using a 9x3 mm breaker plate. The images show that when not using a breaker plate, the fibers become partially orientated (according to Figure 3.6). However, when using the 9x3 mm breaker plate, the fibers become random orientated in certain places (shown with the red circle).

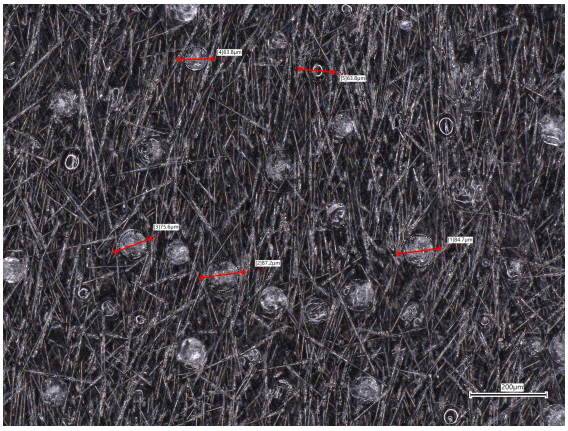

Figure 3.7: No breaker plate (OM 200x)

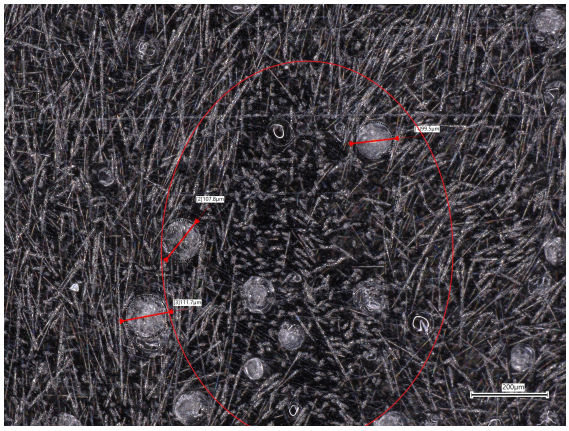

Figure 3.8: 9x3 mm breaker plate (OM 200x)

Figures 3.9 and 3.10 show images of samples cut in the print direction, for a sample where a DFC module was used, and no breaker plate. The images show a similar fiber orientation as when using a breaker plate (see Figure 3.8). However, the location of the ”spiralizing” is somewhat different, as it is located at the edges of the sample. Figure 3.10 shows a more orientated fiber alignment going along the middle of the sample.

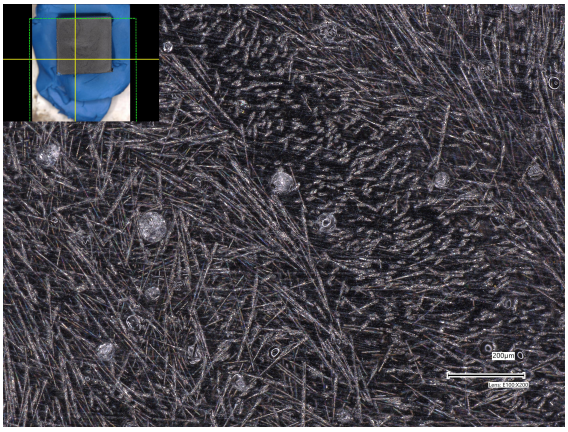

Figure 3.9: DFC, location 1 (OM 200x)

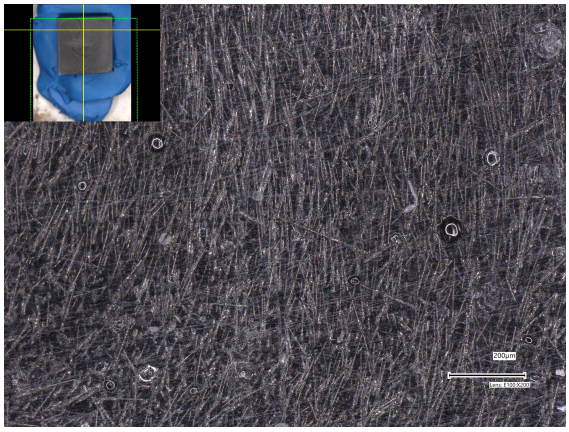

Figure 3.10: DFC, location 2 (OM 200x)

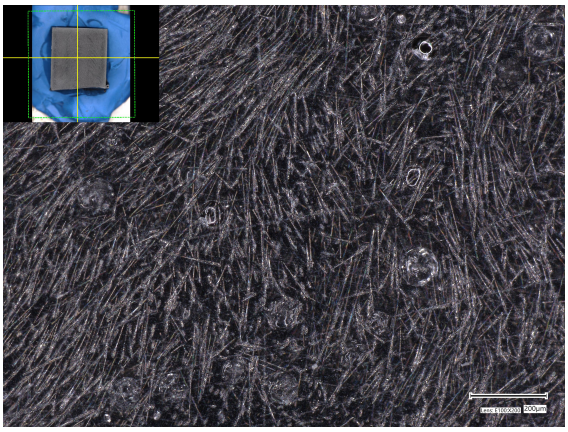

Figure 3.11: DFC and breaker plate loc 1

Figure 3.12: DFC and breaker plate loc 2

The results for the microscopy show that when using no breaker plate or DFC, the fibers tend to be partially orientated in the print direction (see Figure 3.6). When adding a breaker plate (in this case a 9x3 mm breaker plate), the fibers tend to ”spiralize”, causing the fibers to also orientate in the bead direction. When adding a DFC module, the same phenomenon happens as with a breaker plate, however, only on the edges of the bead. Adding a breaker plate as well as a DFC module causes the fibers to become more random orientated (more surfaces where the fibers are directed in the bead direction).

However, these results are relatively localized. Using x-ray tomography, it is expected that the results will give a more global understanding of the fiber orientation.

3.1.2 X-ray Tomography

The X-ray Tomography (Micro CT) machine used in this research is the ”Zeiss Xradio Context MicroCT” (shown in Figure 3.13) at the department of Bio-mechanical engineering at the TU delft. The reason for doing Micro CT is to validate the data gained from optical microscopy. Also, using Micro CT, the global fiber orientation can be better understood.

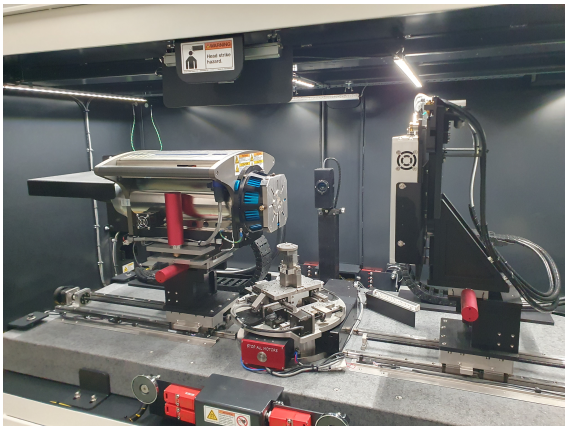

Figure 3.13: Micro CT machine

Figure 3.14: Sample on holder

Two samples are scanned, both made out of PC. The first sample is without the added components (so no breaker plate or DFC module), and the other sample is with the breaker plate (no DFC). Due to the costly operating costs, only two samples where scanned. The samples where prepared as small as possible (approximate 1x1x1 cm) and placed on a holder in front of the source of the machine which dissipates the x-ray beams (Figure 3.14).

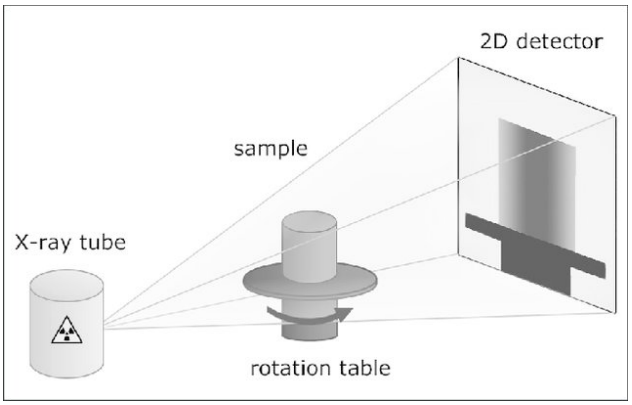

Figure 3.15: Working principle x-ray tomography (micro CT) [20]

The Micro CT scan works by rotating the sample, and acquiring several views from different angles. The x-ray beams pass through the material, and are recorded on the 2D detector (Figure 3.15). The x-ray beams passes with a different intensity depending on the phase of the material (the matrix, fiber and contaminations). The acquired images are then reconstructed to create a 3D image of the structure. The different phases of the material can be separated by tweaking the contrast of the image.

In total, 1923 slices have been made of the 1x1x1 cm cube sample. To reduce the memory usage, slices 500-1000 have been taken, and the image has been cropped. Figure 3.16 shows 3D image of the 2D images stitched together for the sample without breaker plate or DFC. The print and bead direction are respectively Y and Z axis in the image. The images obtained from the Micro CT scans where generated using Dragonfly 2022.2 [Windows]. Comet Technologies Canada Inc., Montreal, Canada; software available at https://www.theobjects.com/dragonfly

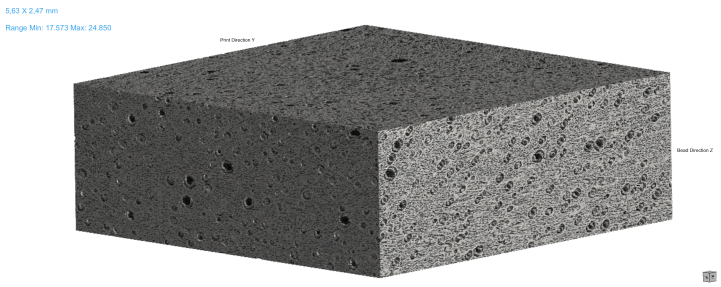

Figure 3.16: Stitched 3D image of micro CT scan

Void content

For determining the void content in an image taken by Micro CT, a similar technique is used as in optical microscopy. The one main difference is that the void content throughout the whole bead direction (Z direction) can be identified, in contrast to optical microscopy, where only one surface is put under the microscope. Figure 3.17 shows a image of an unfiltered cross section of the sample without breaker plate or DFC module.

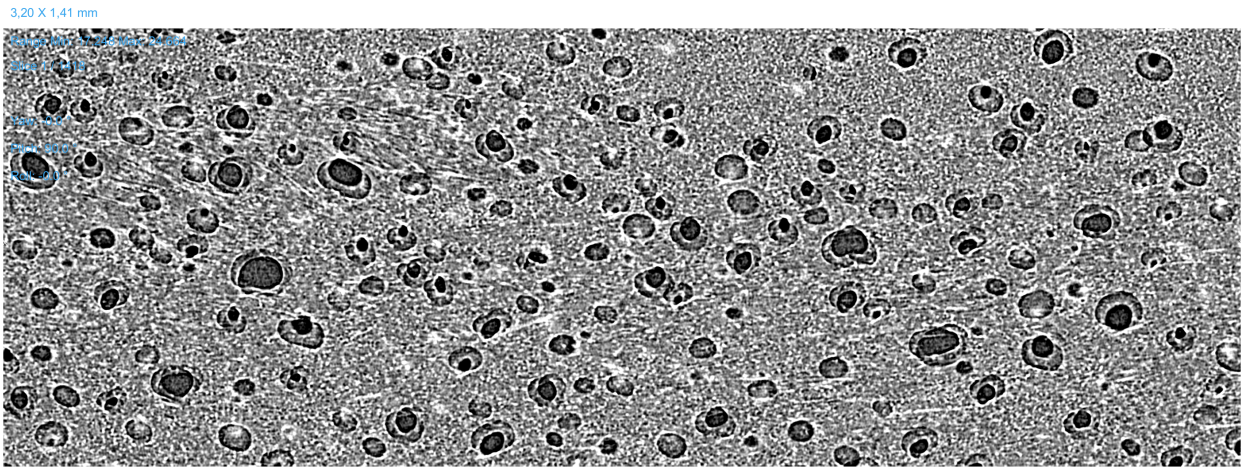

Figure 3.17: Unfiltered cross section showing the voids

The same technique has been used for the micro CT sample with breaker plate.

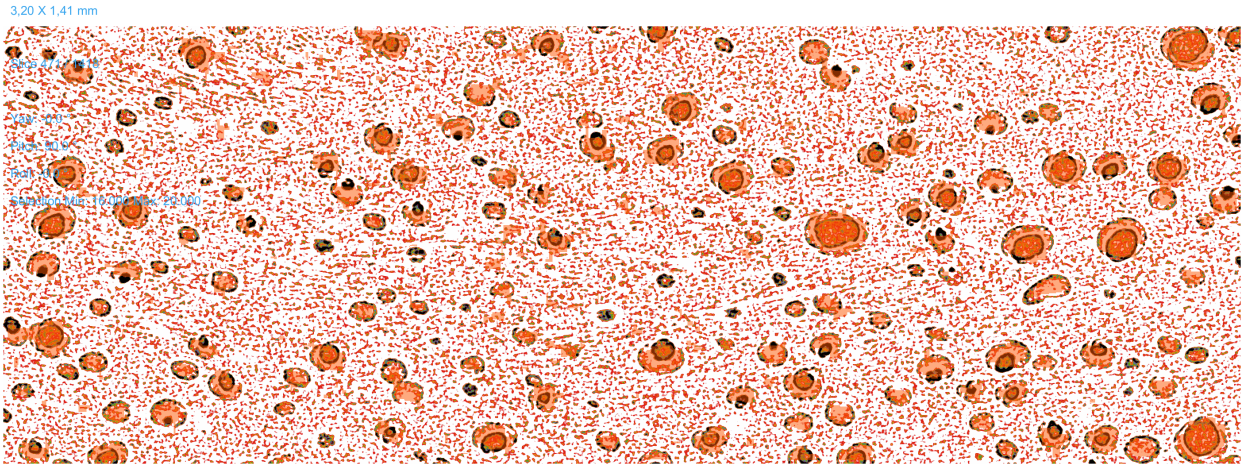

Figure 3.18: Filtered cross section overlapped with original image

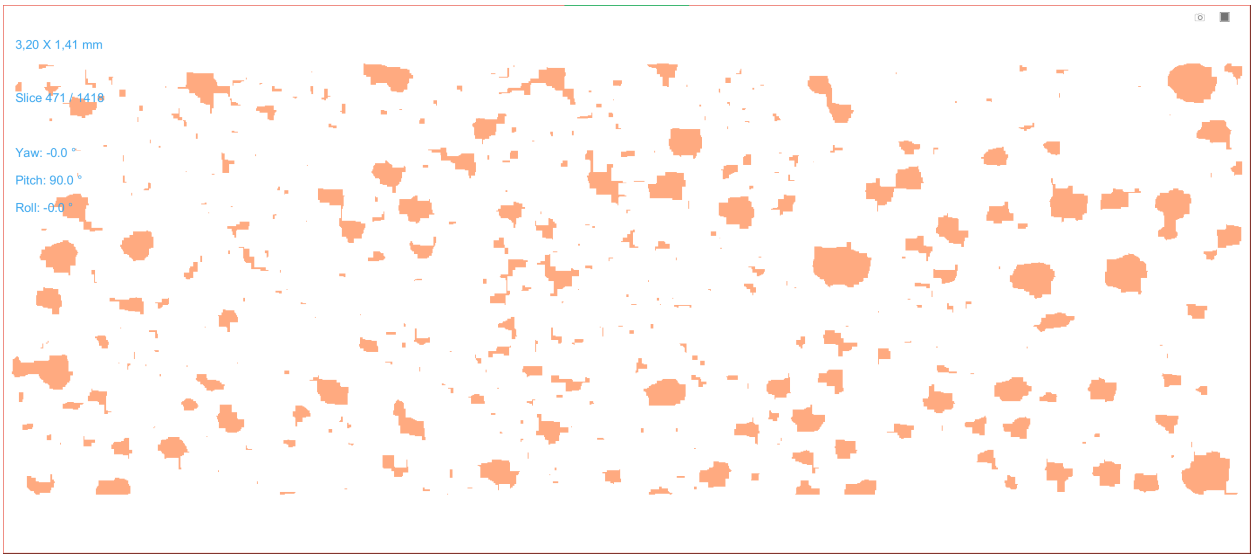

Figure 3.19: Cross section showing only the voids

Figures 3.18 and 3.19 show how the filtering process occurs. First the intensities are filtered to include only the voids. However, during this filtering, other features are usually unintentionally included. Using tools like dilating, eroding and smoothing, the voids can be selected out of the image. This is automatically done for all the slices (each image taken throughout the bead/Z direction). The area content of each slice is determined (shown in Figure 3.20 for both samples).

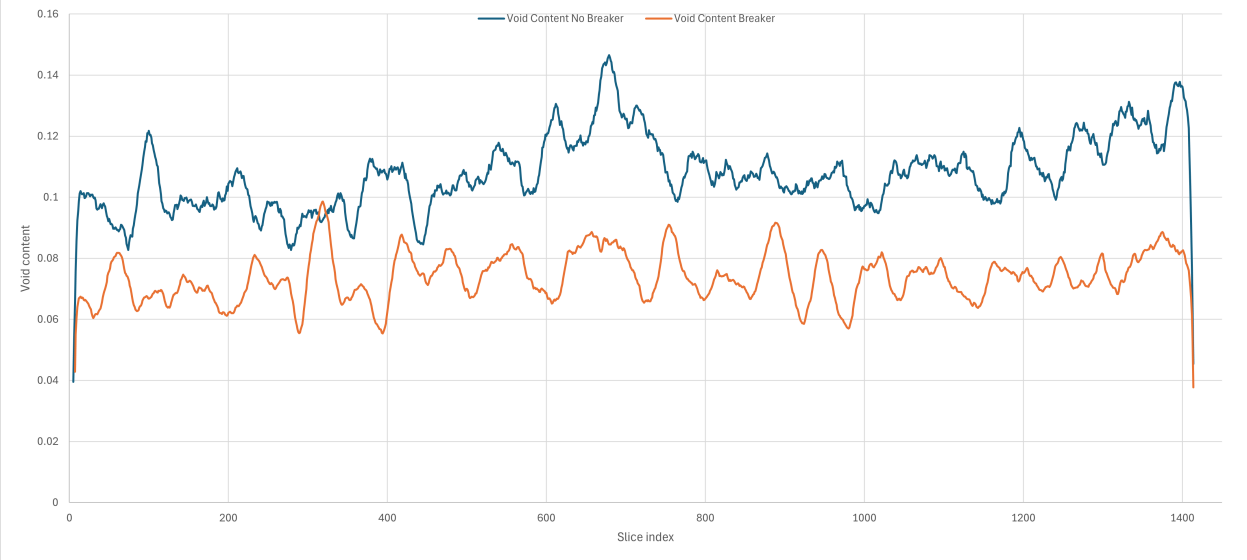

Figure 3.20: Void area content of both samples

Figure 3.20 shows that the sample without breaker plate has an average void content of 10.8%, while the sample with breaker plate has an average void content of 7.4%. Comparing these values to the ones obtained through optical microscopy (7.4% and 5.6%) it can be seen that the void content obtained through micro CT is slightly higher. However, it seems that optical microscopy can give a good approximation on the void content when only looking locally, while micro CT gives a more global approximation of the void content.

Fiber orientation

The fiber orientation can also be identified for more slices, to get a more global understanding. The figures below show the fiber orientation of both samples (left without breaker plate and right with breaker plate).

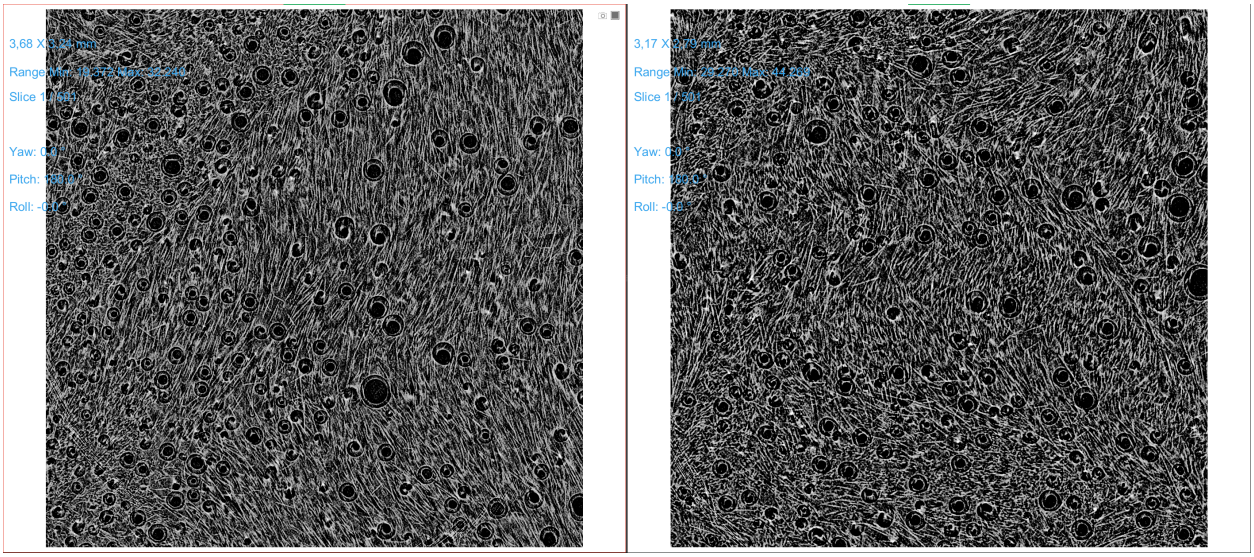

Figure 3.21: Slice one fiber orientation for both samples

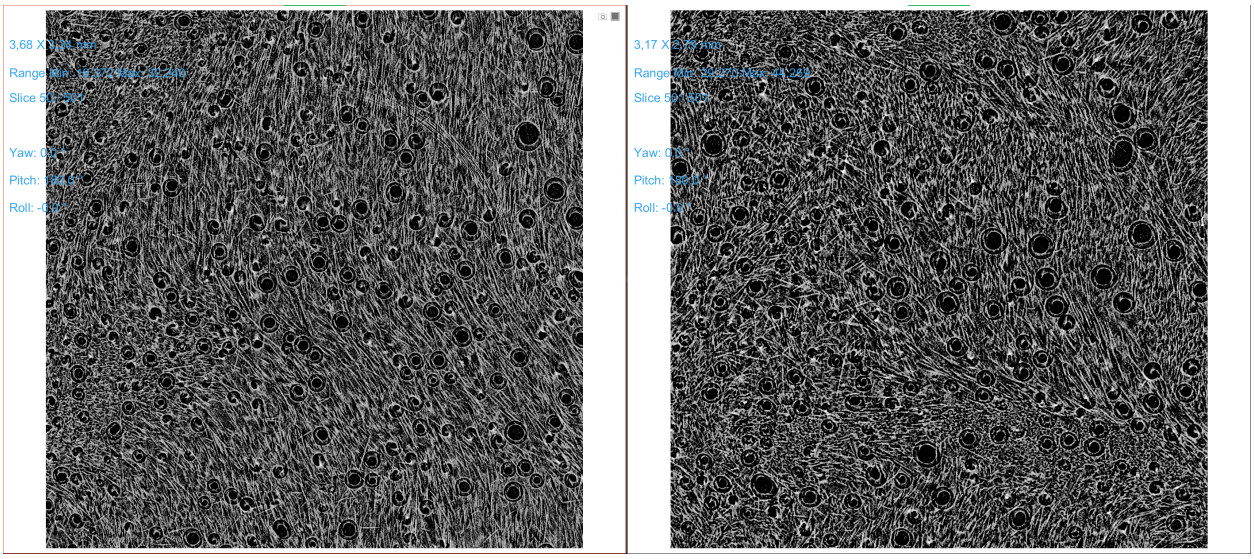

Figure 3.22: Slice 50 fiber orientation for both samples

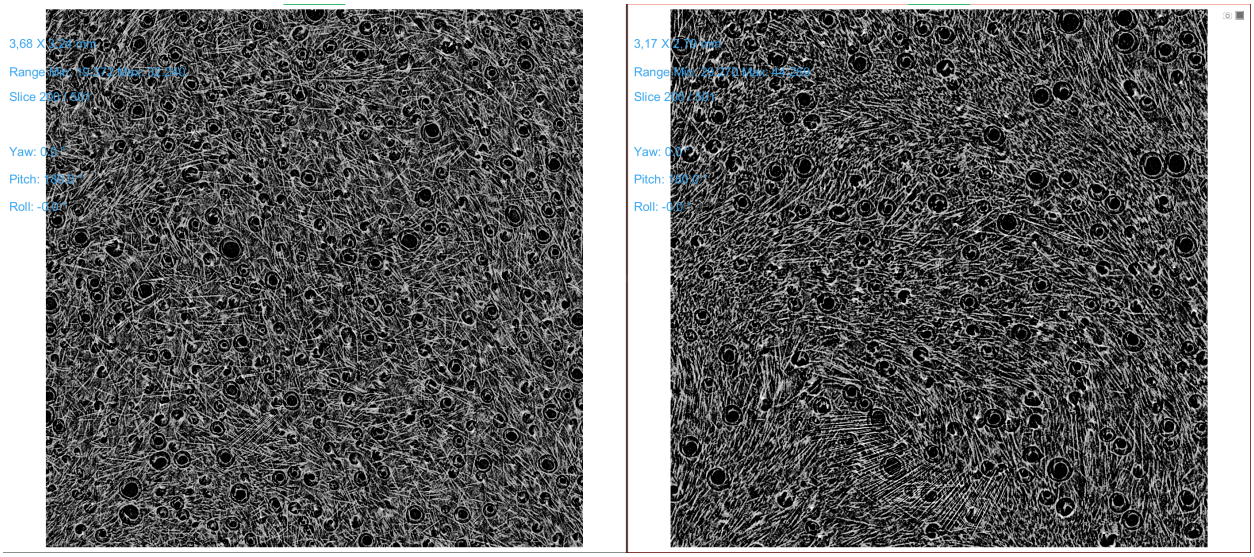

Figure 3.23: Slice 200 fiber orientation for both samples

Figures 3.21, 3.22 and 3.23 shows some images of the fiber orientation of both samples, taken at different slices (also an animation of the change in fiber orientation was made). The figures (and animations) show that the sample without breaker plate has a partial orientation directed in the print direction (Y axis), where all the fibers lie within the same plane. The sample with breaker shows a random orientation, where some of the fibers lie perpendicular to the print plane. This corresponds to what was locally observed in optical microscopy. The conclusion drawn about the fiber orientation in optical microscopy is therefore fair.

3.2 Finite element analysis

This section shows the results gained from Finite Element Analysis. The software used in this research is ”Comsol Multiphysics”. Different material properties have been calculated, all with different coefficients of thermal expansion.

As mentioned before, two options are possible for modeling the properties of the short fiber composite. A RVE model, or averaging the properties across the model, using the analytical models found before (homogenization method). Figure 3.24 shows an example of a RVE model, and here it can be seen how complex the geometry can be. In contrast to continuous fibers, this will not result in a actual representitave model, since the geometry would become so comples, no actual computational time would be preserved. For this reason, field homogenization will be used for the determination of the thermal expansion (equations for SFRP will be used for determining the effective properties in the model).

CTE values as given by the manufacturer, and according to the SFRP formulas are used in the calculations. The CTE values according to the SFRP formulas also include the different fiber orientation (aligned in the print direction, and random orientated). The calculations according to Mori-Tanaka are left out of the FEA calculation (reason for this is explained in the section Discussion). The differences between the datasheet values, aligned fiber orientation and random orientation are presented in this section.

3.2.1 Boundary conditions

In this section the boundary conditions, material properties and made assumptions are shown. Figure 3.25 shows the model being calculated.

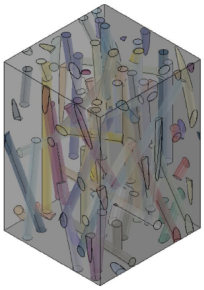

Figure 3.24: Example RVE model [21]

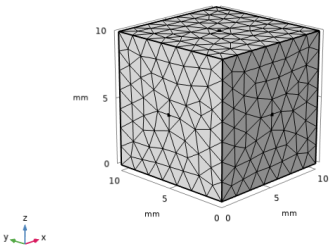

Figure 3.25: Mesh model

It is a simple 10x10x10 mm cube, with the X direction representing the print direction and the Z direction the bead direction. The mesh consists of tetrahedral elements, which are preferred over hexahedral elements for their suitability in complex geometries, which can proof useful for future calculations, such as modeling voids or mold geometries. The cube’s dimensions match the 10 mm extensometer used in thermo-mechanical testing.

In the model, linear elastic behavior has been assumed, as the forces acting on it are sufficiently low and the temperature remains below the glass transition temperature. Additionally, the pressure acting on the model has been disregarded, as it is also sufficiently low and is not expected to influence the model’s thermal expansion. The effect of pressure will be discussed in the thermo-mechanical testing section.

The model is given an initial value of 20 degree Celsius. To simulate the transfer of heat in the oven/autoclave, a convective heat transfer coefficient of 25 W/($m^2 \cdot K$) has been used. This is a typical value to simulate the air flow in an oven.

The CTE values used in the FEA calculations are shown in Table 3.3. For the random orientated fibers, according to the SFRP formulas and theory, the coefficient of thermal expansion becomes isotropic. The values used to determine the CTE values according to the SFRP formulas where gained from "CES Edupack".

CTE	PC datasheet	PEI datasheet	PC aligned	PEI aligned	PC random	PEI random
CTE X [1/K]	10.88E-6	7.58E-6	19.48E-6	15.68E-6	42.17E-6	32.34E-6
CTE Z [1/K]	110.7E-6	74.87E-6	64.86E-6	49.01E-6	42.17E-6	32.34E-6

Table 3.3: CTE values used in FEA according to datasheet and SFRP formulas

Furthermore, the calculations require additional material data. The used values for the calculations are shown in Table 3.4.

Parameter	Symbol	Value	Unit	Notes
Fiber modulus	E_f	260×10^9	Pa	Range: 225-260 GPa
Fiber CTE	α_f	-2×10^{-6}	1/K	Range: -2 to 0.3 $\times 10^{-6}$
Fiber Poisson's ratio	v_f	0.1	-	Range: 0.01-0.2
Matrix modulus	E_m	2.44×10^9	Pa	Range: 2.32-2.44 GPa
Matrix CTE	α_m	120×10^{-6}	1/K	Range: 120-125 $\times 10^{-6}$
Matrix shear modulus	G_m	0.85×10^9	Pa	Range: 0.829-0.872 GPa
Matrix Poisson's ratio	v_m	0.4	-	Range: 0.391-0.407
Fiber length	l	75×10^{-6}	m	-
Fiber radius	r_f	3.5×10^{-6}	m	-
Fiber center-to-center distance	R	10×10^{-6}	m	-
Fiber volume fraction	v	0.2	-	-
Effective Poisson's ratio	v_{12}	0.2	-	Composite property

Table 3.4: Material properties (PC) used in the composite CTE analysis

The Y-direction is ignored in the thermal expansion analysis because the X (print direction) and Z (bead direction) dominate expansion behavior. In aligned fiber orientated composites, expansion in Y is nearly identical to X, while in random fiber orientated composites, expansion (XYZ) is nearly isotropic. Focusing only on X and Z simplifies simulations and measurements.

3.2.2 Results from FEA

This section shows the results gained from doing FEA. Figures 3.26 - 3.31 show the dimensional change (total displacement) of the model under an applied temperature.

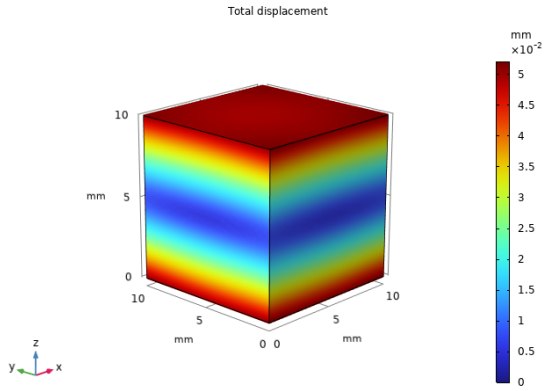

Figure 3.26: PC according to data sheet

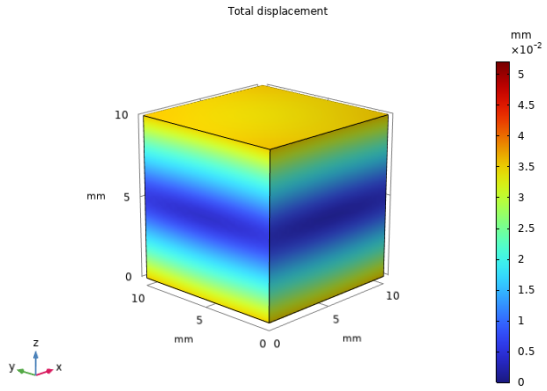

Figure 3.27: PEI according to data sheet

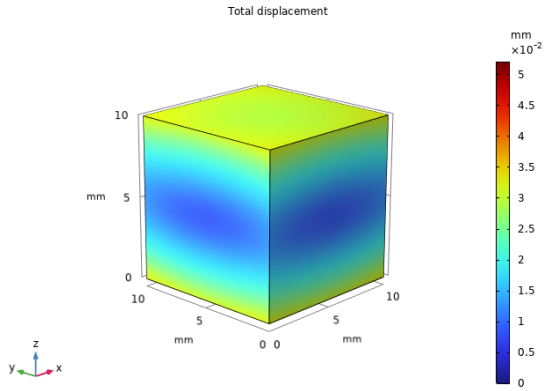

Figure 3.28: PC aligned fibers

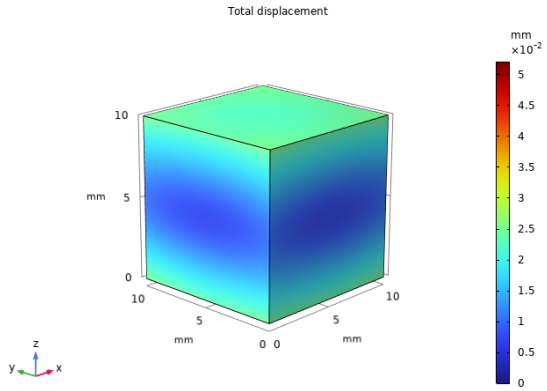

Figure 3.29: PEI aligned fibers

The model was calculated to simulate being in an oven, untill heated up to circa 100 degrees Celcius. The results show the maximum thermal expansion, reached in the simulation (after two minutes). The thermal expansion of all the materials are also shown in Figures 3.32 and 3.33, where the thermal expansion is plotted against the temperature.

The results show that for the displacement in the print direction (x displacement), the values are relatively higher for random orientated fibers. The result for the displacement in the bead direction (z displacement) show that the displacement remains the same for the random orientated fibers (isotropic behavior), and the displacement for the aligned fibers increases. These results are validated using thermo-mechanical testing.

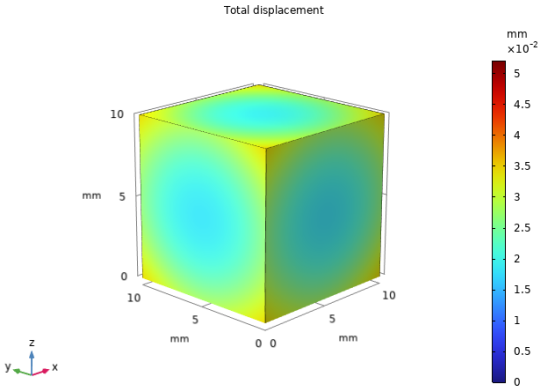

Figure 3.30: PC random fibers

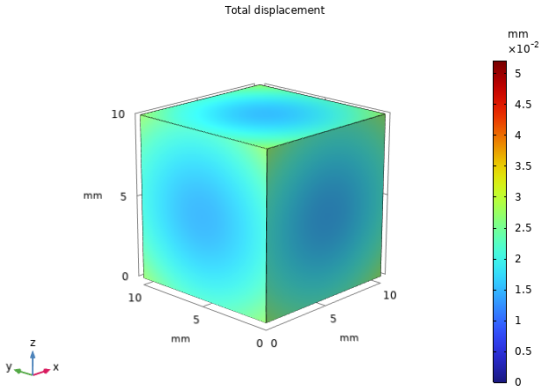

Figure 3.31: PEI random fibers

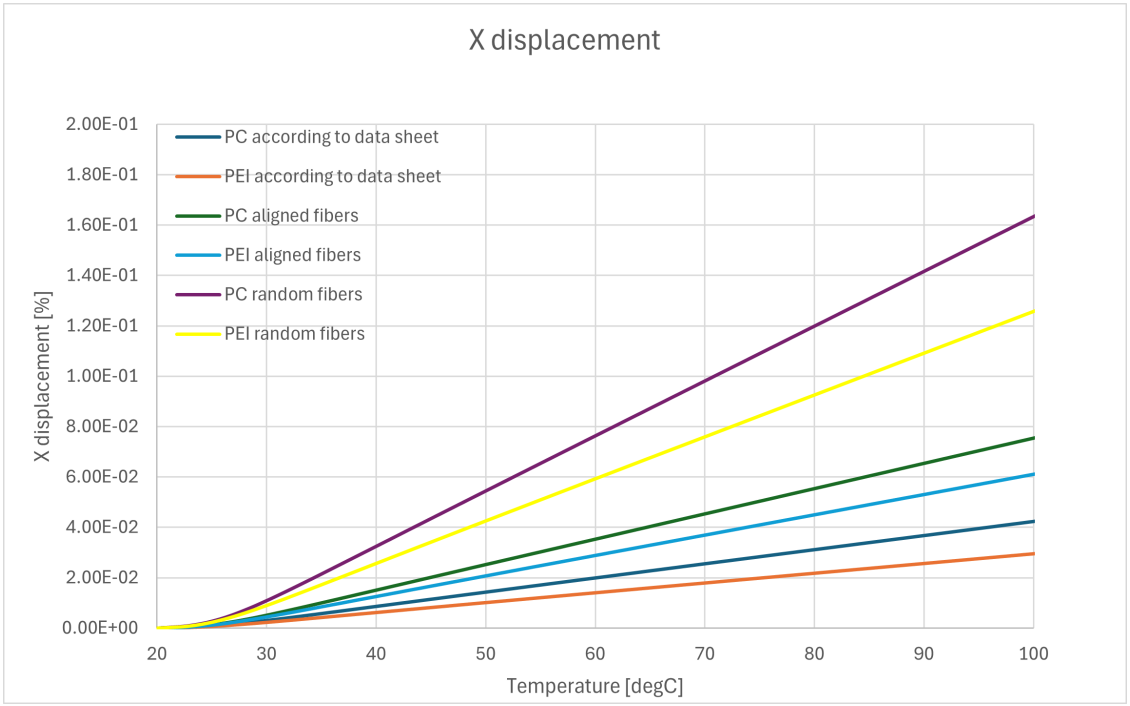

Figure 3.32: X displacement

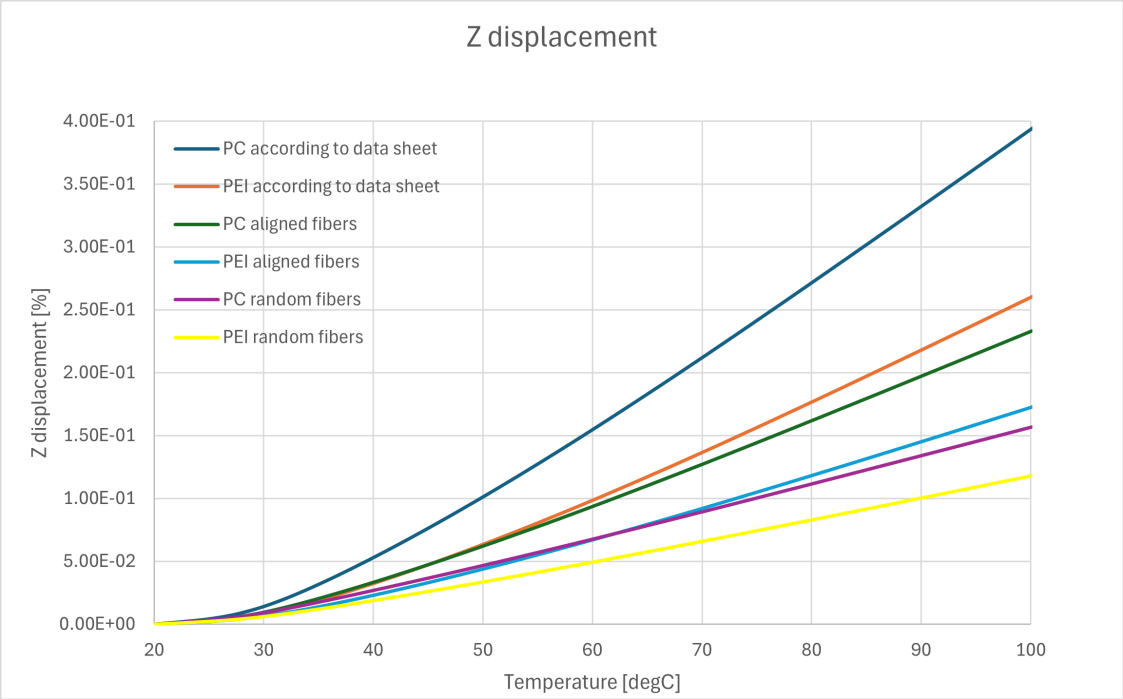

Figure 3.33: Z displacement

Besides the fiber orientation, the void content has also been investigated. Using the material data given by the manufacturer, a cube model containing a void with a spherical shapes has been modeled, and calculated for a range of void contents. For this calculations, some assumptions where made, such as the assumption that the voids are all spherical. From the microscope images, it can be seen that most of the voids take the shape of an ellipsoid. Also, for the calculation, it has been assumed that all the voids have the same radius. From Table 3.1 it can be seen that this also ranges from a minimal and maximum value. For this calculation, a void diameter of 0.1 mm has been assumed. The range of void content that has been investigated are 5%, 10% and 15% (shown in Figures 3.34 and 3.35). The models where created using the open source software "Gmsh" [22]. Using a Python code, spheres with a specific dimension where randomly placed inside a cube according to a specific volume fraction of voids.

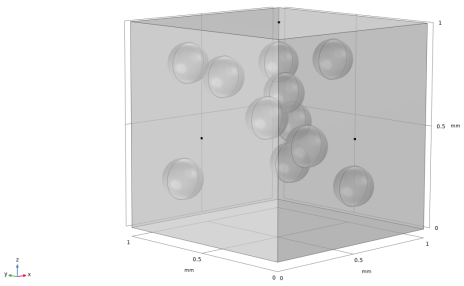

Figure 3.34: Cube with 5% void content

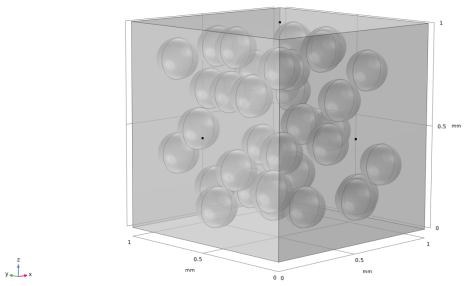

Figure 3.35: cube with 15% void content

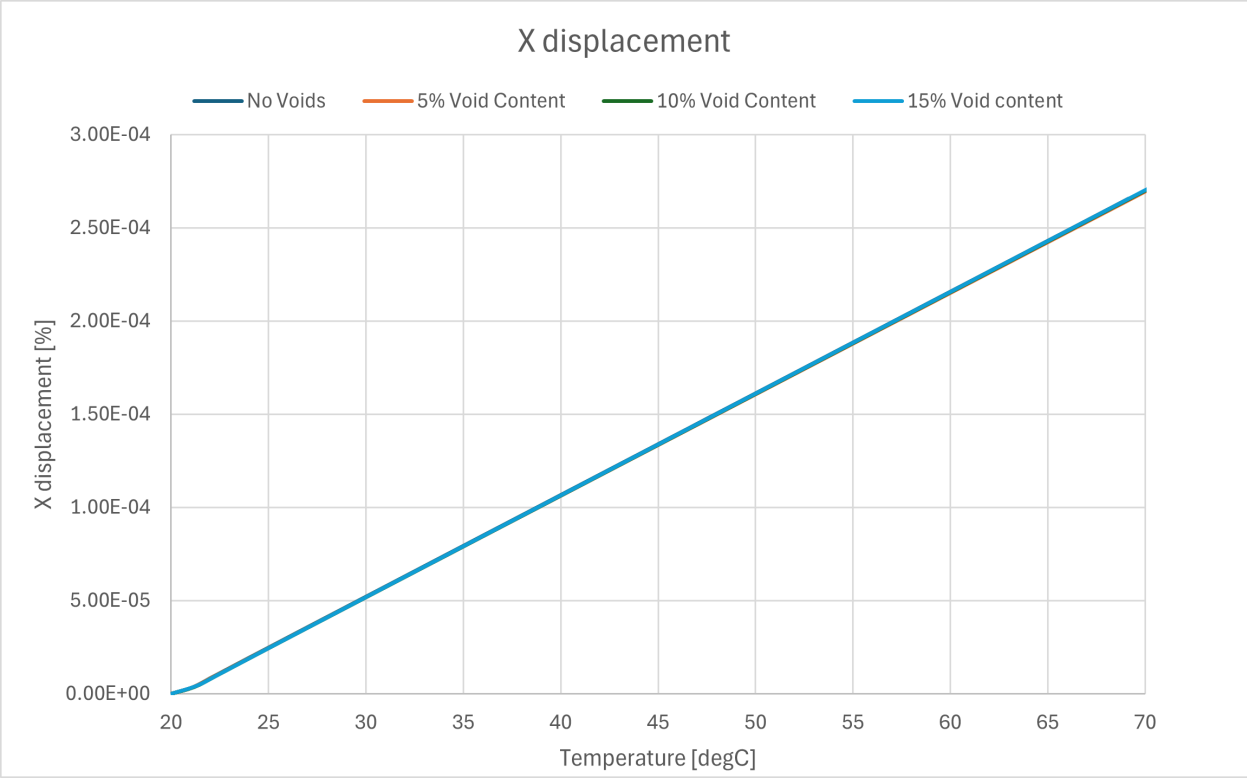

Figure 3.36: X displacement with different void content

Figure 3.36 shows the difference in the void content on the X displacement of the cube. Here it can be seen that the influence of the voids are minimal on the thermal expansion (an increase of circa 5%). The same effect was seen for the Z displacement.

It is expected that the thermal expansion is not that much influenced by voids due to the fact that thermal expansion is mainly governed by the CTE value of the material. The properties mainly affected by voids are the mechanical properties (reduced strength and weaker structure for the model with voids), and the thermal conductivity. The model with voids will have a lower thermal conductivity, since the air inside the voids are relatively not a good conductor of heat compared to the solid matrix.

In the models the voids are randomly distributed in the cube. This can create localized stress concentrations, making the model more inclined to failure at these locations under load. Also the randomness of the voids create a unpredictable heat transfer path. However, since the voids are randomly scattered in the cube (and small compared to the cube), the expansion still remains uniform. Figures A.1 and A.2 in the Appendix show the difference in the stress distribution for the model without voids and the model containing 15% voids, conforming the theory about localized stress concentrations.

3.3 Thermo-mechanical testing

This section describes the thermo-mechanical testing, and the results gained from the testing. The machine used for measuring the thermal expansion is Instron E20000 at the department of Material Science & Engineering at the TU Delft (Figure 3.37).

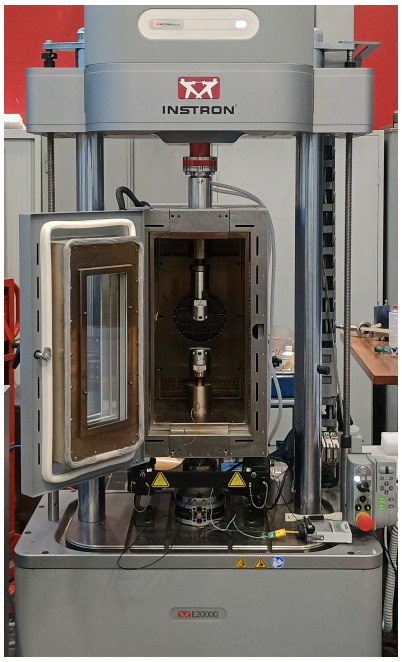

Figure 3.37: Instron E20000 DMA machine

Figure 3.38: Working principle DMA

The thermal expansion is measured by placing a cube in between the actuators of the Dynamic Mechanical Analyzer (shown in Figure 3.38), and attaching an extensometer (measurement device to measure the displacement) on the side of the cube. In addition to the extensometer, a thermocouple is placed on the opposing side of the cube, to measure the current temperature of the cube inside the oven.

Five tests are performed on each direction (X and Z direction) of the sample. Also an additional test has been performed to identify the difference when adding pressure and no pressure. This is done by applying a force corresponding to 6 bar. However, it should be noted that since not all sides of the cube are loaded (only top side), the test with pressure is only an indication of the difference in thermal expansion.

Figures A.3, A.4, A.5 and A.6 in the Appendix show the displacement in the X and Z direction of the performed DMA tests. Here it can be seen that when not using a breaker plate or DFC, the CTE values in the x-direction are relatively lower than the sample with breaker plate. The z-direction shows similar values for both of the samples. So a difference when using the breaker plate and not can definitely be observed. The difference between the results gained from DMA and FEA are further discussed in the section Discussion.

The effect of pressure on the cube has also been investigated using the DMA test method. In the test results shown in Figures A.3, A.4, A.5 and A.6 in the Appendix, a constant force of 10 N on the sample has been applied. This is just a clamping force, to hold the sample in place, and is a negligible force compared to the material properties. For the sample without breaker plate, an additional test has been performed for testing the effect of pressure. This has been done by applying a force on the top side of the cube, corresponding to 6 bar (0.6 N/mm^2 * 16 mm * 16 mm). However, this test did not give reliable results. The reason for this is that the setup of the test is a area load. This corresponds to a non-uniform stress distribution, in contrast to an uniform pressure, where the pressure would lead to a "near-isotropic" compression.

To still check for effect of pressure, a simple calculation has been done. This has been done according to Equation 3.1. ΔV is the change in volume, P is the applied pressure and K is the bulk modulus (material property). The bulk modulus was determined using values given by the manufacturer (can be calculated using Equation 3.2).

$$\Delta V = -\frac{PV}{K} \tag{3.1}$$

$$K = \frac{E}{3(1-2v)} \tag{3.2}$$

Since the bulk modulus of the Z direction is the lowest (highest thermal expansion in the Z direction), this will give the maximum change in volume. Substituting the values, a volumetric change of approximately -4.6×10^{-4} is obtained. This corresponds to a shrinkage of 0.046% in volume due to the applied pressure (6 bar). The effect of pressure is negligible compared to the thermal expansion, and is therefore not further investigated.

To validate if the test method is correct and produces reliable results, an additional test has been performed on an Aluminum 7075 sample. These results are shown in Figure A.7 in the Appendix. These results show an initial non-linear expansion of the material, and then linear expansion. The expansion results do relatively match the results gained from FEA. Aluminum 7075 is a high-strength alloy that can exhibit residual stresses from specific manufacturing processes (like extrusion or machining). It is expected that the non-linearity of the expansion rises from the relaxation of the residual stresses in the material.

Chapter 4

Discussion

This section discusses the results gained from Finite Element Analysis and Thermo-mechanical testing. For FEA, the homogenization technique has been used to determine the overall material properties of the model. This included the analytical model based on the SFRP equations shown in Section 2.1.1. However, in Section 2.1.1, another model (M-T model) was presented as a possible way to determine the coefficient of thermal expansion for short fiber composites.

The main reason for not including the M-T model is the way the analytical model determines the coefficient of thermal expansion. The main differences between the two analytical models are the orientation averaging and anisotropic representation of the material. The M-T model is well suited for materials with aligned fibers and can capture the effective properties of the material, while the SFRP models are also suited for specific orientations like partial and random orientated fibers. For these reasons only the analytical SFRP model has been used to determine the CTE values.

The CTE values determined by the analytical model shows a higher CTE value than the values provided by the manufacturer. This could be due to the idealized assumptions in the model. The model assumes perfect bonding between the fibers and matrix, an uniform fiber distribution and resulting in an uniform stress transfer between the fibers and matrix. However, the values provided by the manufacturer where determined by doing thermo-mechanical testing using the TMA machine described in Section 2.1.3. This usually accounts for more real-world effects.

The results gained from thermo-mechanical testing (using DMA) compared to the results gained from FEA are shown in Figures A.3, A.4, A.5 and A.6 in the Appendix. The results show that the data acquired from DMA do not precisely match the data acquired from FEA. This is logical since FEA makes ”perfect world” assumptions, like ignoring the bonding between the fibers and matrix, non-uniform heating due to the fiber distribution, and other assumptions. What is more interesting is the trend how the X and Z displacement changes when using components (breaker plate) that influence the fiber orientation, and to see how the fiber orientation influences the thermal expansion.

The images acquired from optical microscopy and x-ray tomography show that when adding a breaker plate component, it results in a more random fiber orientation. The breaker plate is expected to increase the randomness of fiber orientation by introducing additional shear and turbulence, disrupting the alignment of fibers with the flow direction. Without the breaker plate, the images show a more partial orientation of the fibers. So according to the analytical models, the results of the sample without breaker plate should give a relatively higher Z CTE values and a relatively low X CTE value. When using the breaker plate, the results should give values corresponding to a random fiber orientated sample. According to the CTE values gained from the analytical model, the CTE values of the X and Z direction should be very similar, and in between the minimum and maximum CTE value for aligned fibers.

The results shown in the Figures show that for the sample without breaker plate, the X direction has a lower CTE value than the Z direction (with the exception of the first two tests). This corresponds to what is expected according to the analytical models. However, it seems that the values gained from FEA do not really match the results gained from thermo-mechanical analysis. The interesting trend that appears is that the CTE values (according to the thermo-mechanical testing) is slightly higher when using a breaker plate. This matches the theory according to the analytical model, that the CTE values are higher when the fibers are random orientated in the X-direction. The results for the Z-direction show that there is not a huge difference in the CTE values between the samples with and without breaker plate. The one thing that can be observed is that the first test, for the sample with breaker plate, shows a relatively low CTE value. After the initial test, all the CTE values become similar and relatively the same as the sample without breaker plate. This could be due to the fact that the sample is annealed in the first test.

For the thermo-mechanical testing, five tests per side has been performed. It seems that FEA still proofs to be a useful tool for predicting trends in CTE behavior. While there are some discrepancies between the FEA results and the thermo-mechanical analysis, FEA still provides valuable insights into the influence of fiber orientation on thermal expansion. The observed deviations could be attributed to assumptions in the modeling process, material property variations, or limitations in boundary conditions. Nevertheless, FEA remains a relatively accurate method for approximating material behavior and serves as a complementary approach alongside experimental analysis. Figure 4.1 shows an example of a whole mold calculated using FEA, and using these images, weak spots in the model can be identified and improved in the future.

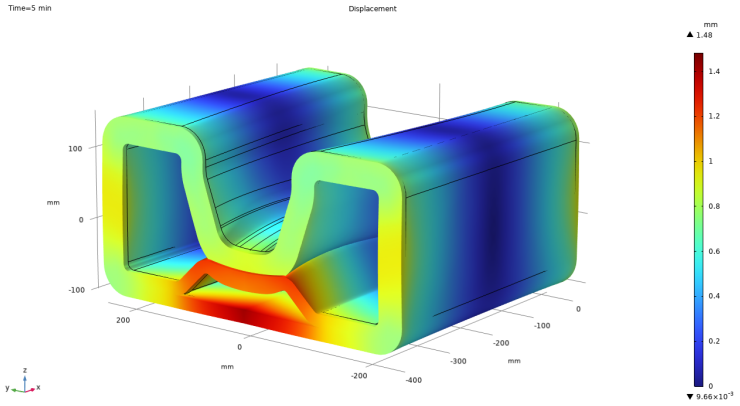

Figure 4.1: Example of total displacement for whole mold

Chapter 5

Conclusion

This study demonstrates that finite element analysis (FEA) is a reliable method for predicting trends in the coefficient of thermal expansion (CTE) of fiber-reinforced polymer composites. While discrepancies exist between FEA and experimental results, FEA provides valuable insights into the impact of fiber orientation on thermal expansion. Deviations likely stem from modeling assumptions, material property variations, and boundary condition limitations, underscoring the need for further refinements.

A key finding is the influence of the breaker plate on fiber orientation and CTE. Optical microscopy and x-ray tomography confirm that breaker plates promote a more random fiber orientation, resulting in more uniform but slightly lower CTE values in the primary X direction. Analytical models support this trend, indicating that random fiber distribution yields more isotropic thermal expansion behavior.

Additionally, the short fiber-reinforced polymer (SFRP) model effectively captures CTE trends despite differences in absolute values from experimental data. The SFRP model was favored over the Mori-Tanaka (M-T) model due to its ability to account for partial and random fiber orientations, which better reflect the processing effects of breaker plates and the resulting extrusion behavior in 3D-printed composites.

Void content was found to have a minor but measurable impact, increasing CTE by approximately 5% due to reduced stiffness and thermal insulation effects. However, fiber orientation remains the dominant factor influencing thermal expansion.

FEA enables the identification of weak points in structural design, allowing for optimization of fiber orientation and material composition to improve thermal stability. This capability is especially valuable for large-scale 3D-printed molds requiring dimensional accuracy during autoclave cycles.

While further testing could be done to refine CTE predictions and validate FEA accuracy, implementing breaker plates to achieve controlled fiber orientation and enhanced isotropy is an effective strategy for tailoring thermal expansion properties. Future work should focus on improving experimental repeatability and enhancing analytical and computational models, particularly for large-scale applications. Investigating the combined effects of void distribution and fiber orientation could lead to more accurate predictions and improved material performance.

Chapter 6

Recommendations

Based on the results and conclusions of this study, the following recommendations are proposed:

1. **Improve Finite Element Analysis (FEA) Models**
   More accurate material properties and better boundary conditions could be included in FEA to reduce differences between simulations and experiments.

2. **Optimize fiber orientation control**
   Since fiber orientation affects thermal expansion, changes in the manufacturing process, such as using different breaker plates (or other additional components), should be tested to achieve better material properties.

3. **Increase experimental testing**
   More tests could be done on different samples to improve the reliability of the results and verify the accuracy of the models used in this study.

4. **Study the effect of voids**
   Although voids had a small effect on thermal expansion, their influence combined with fiber orientation could be studied further for better material/model design.

5. **Apply to Large-Scale models**
   The findings could be tested on full-size 3D-printed molds used in real applications to confirm the accuracy of the models and experiments.

These recommendations cam help improve the accuracy of thermal expansion predictions, optimize material performance, and make FEA a more reliable tool for analyzing 3D-printed fiber-reinforced composites.

Appendix A

Appendix

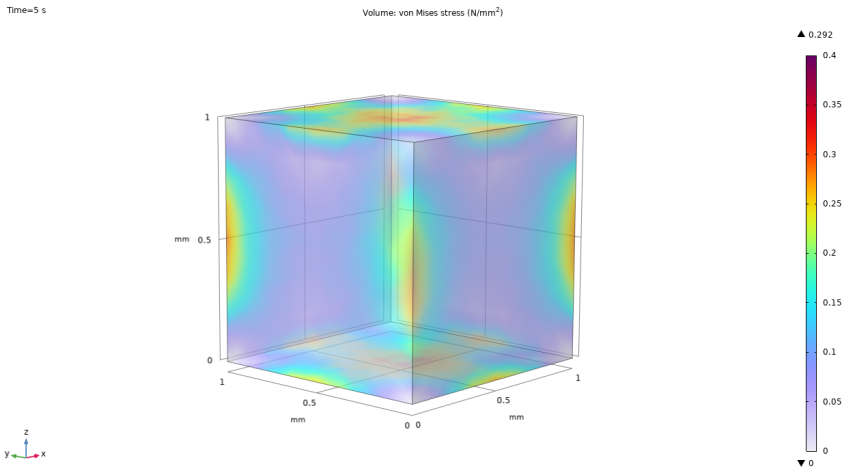

Figure A.1: Stress distribution for model without voids

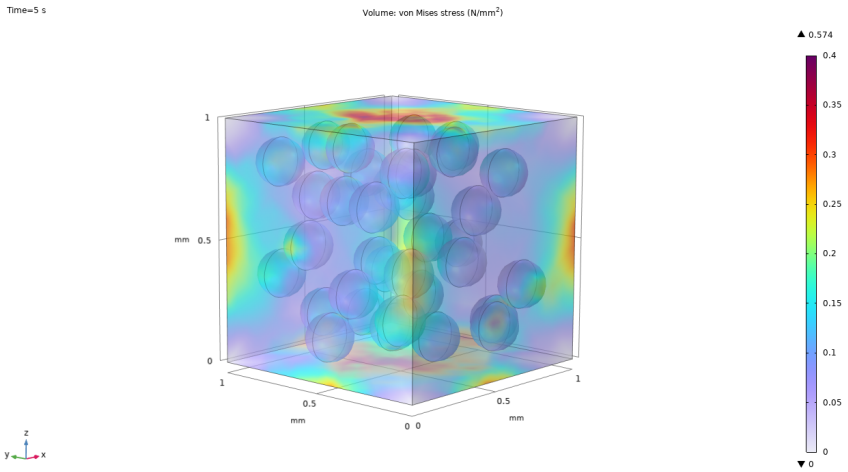

Figure A.2: Stress distribution for model with 15% voids

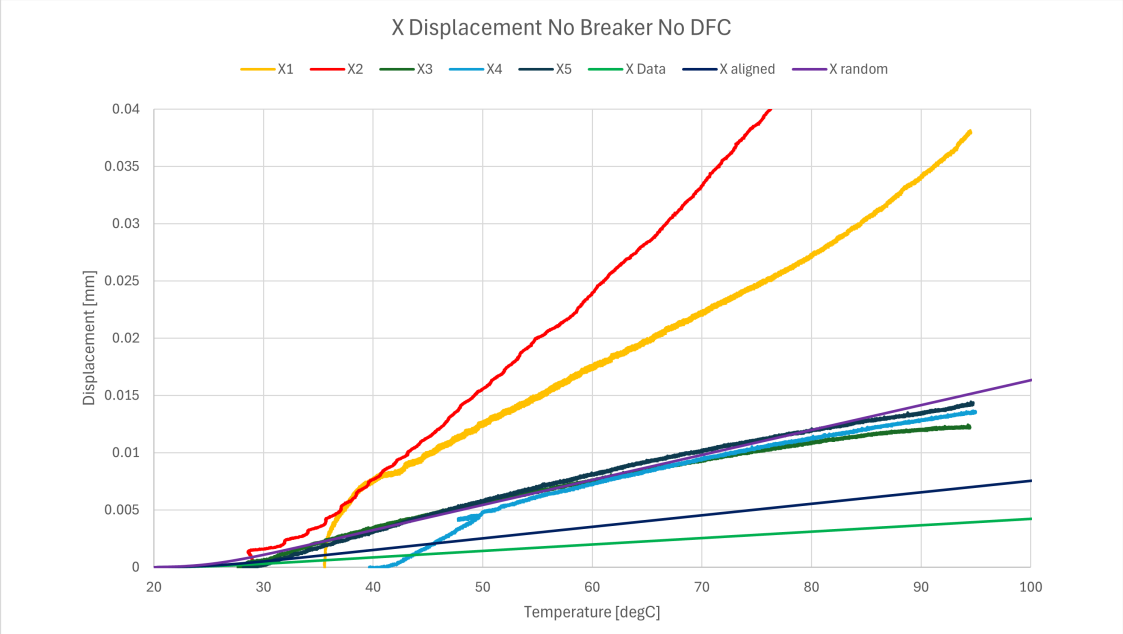

Figure A.3: DMA and FEA results for X direction no breaker no DFC sample

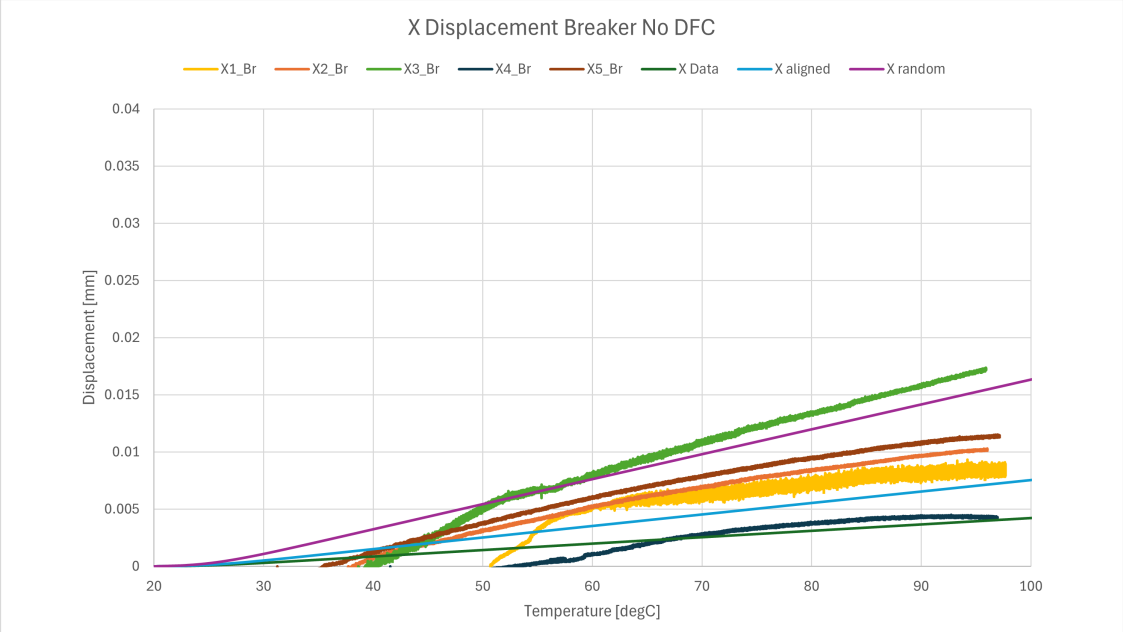

Figure A.4: DMA and FEA results for X direction with breaker no DFC sample

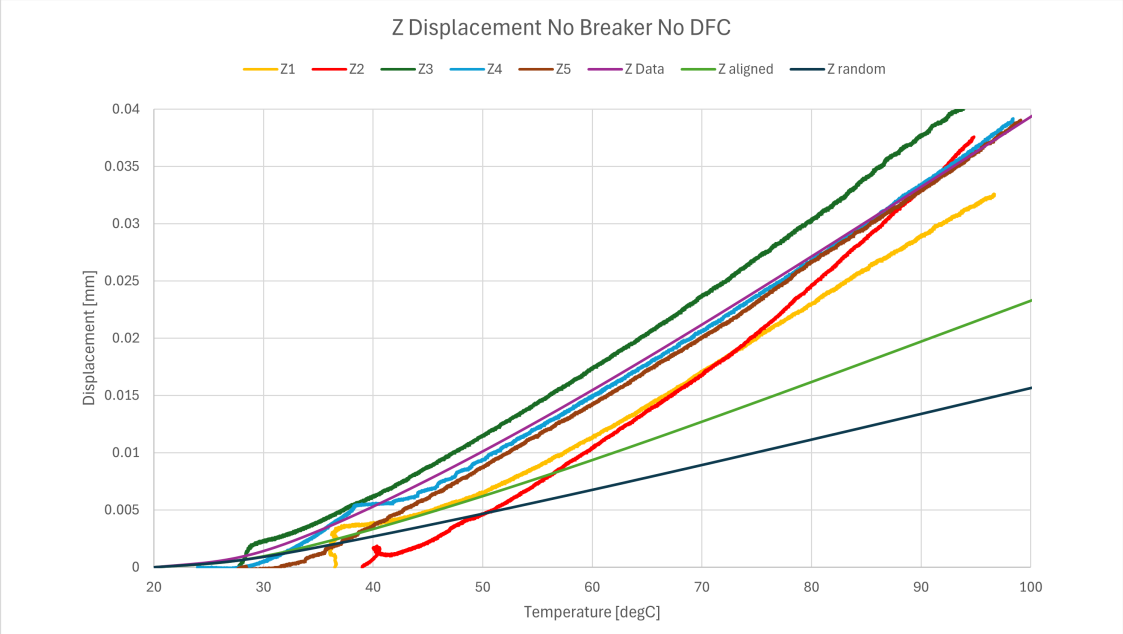

Figure A.5: DMA and FEA results for Z direction no breaker no DFC sample

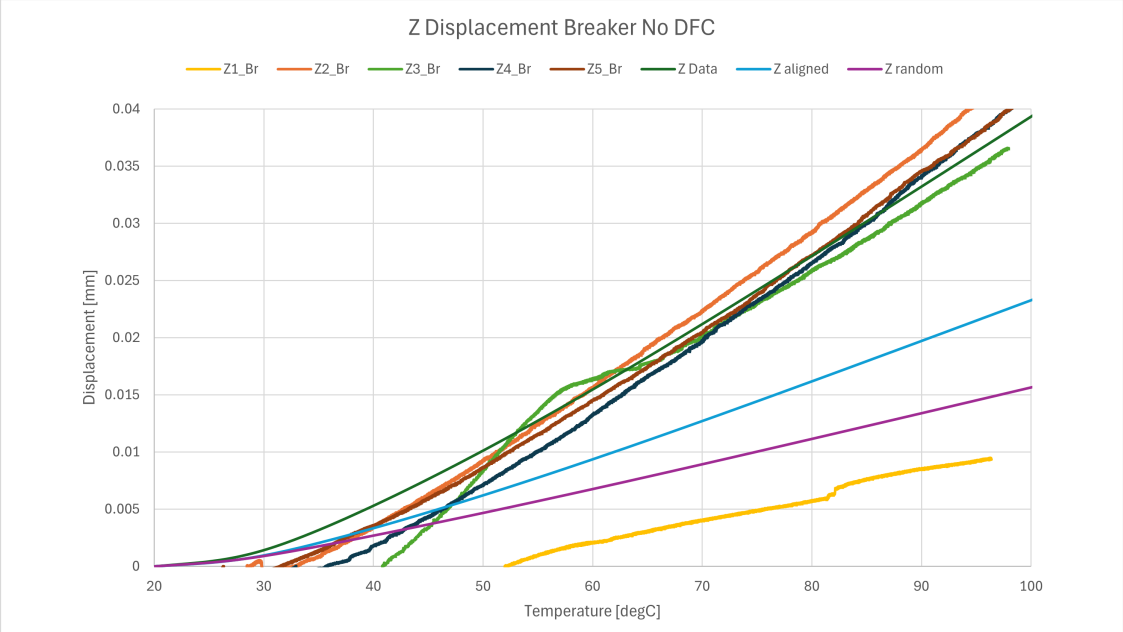

Figure A.6: DMA and FEA results for Z direction with breaker no DFC sample

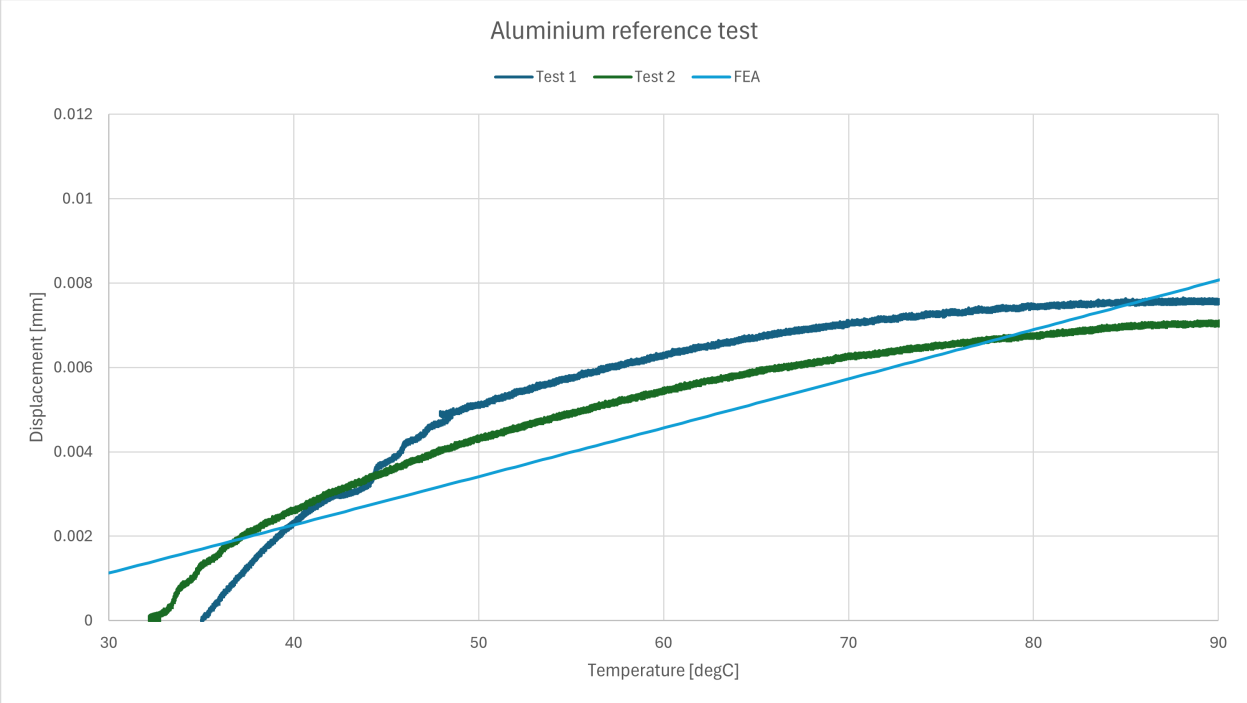

Figure A.7: DMA results of reference test Aluminum 7075 and FEA

Bibliography

[1] N. Saba and M. Jawaid, "A review on thermomechanical properties of polymers and fibers reinforced polymer composites," *Journal of Industrial and Engineering Chemistry*, vol. 67, pp. 1–11, 2018.

[2] L. W. McKeen, "Chapter 7 - polyimides," in *Fatigue and Tribological Properties of Plastics and Elastomers (Second Edition)* (L. W. McKeen, ed.), Plastics Design Library, pp. 149–173, Oxford: William Andrew Publishing, second edition ed., 2010.

[3] *Perspective of polycarbonate composites and blends properties, applications, and future development: A review*, pp. 393–424. Elsevier, 1 2022.

[4] A. Europe, "Dahltram i-350cf supplemental data sheet," 2023. Retrieved from `https://www.airtech.lu`.

[5] Q. Wang, W. ly, W. Zhu, Q. xu, and Y. Ke, "Design optimization of molds for autoclave process of composite manufacturing," *Journal of Reinforced Plastics and Composites*, vol. 36, p. 073168441771826, 07 2017.

[6] A. Patel and M. Taufik, "Extrusion-based technology in additive manufacturing: A comprehensive review," *Arabian Journal for Science and Engineering*, vol. 49, 12 2022.

[7] P. G. Lafleur and B. Vergnes, *Single-Screw Extrusion*, ch. 3, pp. 37–108. John Wiley Sons, Ltd, 2014.

[8] P. J. Hines, S.-W. Tsuib, P. D. Coatesb, I. M. Warda, and R. A. Ducketta, "Measuring the development of fibre orientation during the melt extrusion of short glass fibre reinforced polypropylene," 1997.

[9] The Editors of Encyclopedia Britannica, *thermal expansion*. Aug. 2024.

[10] "Micromechanics analysis for thermal expansion coefficients of three-phase particle composites," *Archive of Applied Mechanics*, vol. 89, pp. 1641–1654, 8 2019.

[11] S.-Y. Fu, B. Lauke, and Y.-W. Mai, "8 - thermal conductivity and expansion of short fibre reinforced polymer composites," in *Science and Engineering of Short Fibre Reinforced Polymer Composites* (S.-Y. Fu, B. Lauke, and Y.-W. Mai, eds.), Woodhead Publishing Series in Composites Science and Engineering, pp. 184–205, Woodhead Publishing, 2009.

[12] L. Wan, Y. Ismail, C. Zhu, P. Zhu, Y. Sheng, J. Liu, and D. Yang, "Computational micromechanics-based prediction of the failure of unidirectional composite lamina subjected to transverse and in-plane shear stress states," *Journal of Composite Materials*, vol. 54, 04 2020.

[13] Graspengineering, "Different types of FEA elements / How to decide the element type," 8 2020.

[14] T. LaForce and Stanford, "PE281 Finite Element Method course notes," tech. rep., 4 2006.

[15] J. James, "Chapter 7 - thermomechanical analysis and its applications," in *Thermal and Rheological Measurement Techniques for Nanomaterials Characterization* (S. Thomas, R. Thomas, A. K. Zachariah, and R. K. Mishra, eds.), Micro and Nano Technologies, pp. 159–171, Elsevier, 2017.

[16] M. J. Pomeroy, "Thermal analysis techniques for technical ceramics and glasses," in *Encyclopedia of Materials: Technical Ceramics and Glasses* (M. Pomeroy, ed.), pp. 676–688, Oxford: Elsevier, 2021.

[17] M. Hunkel, H. Surm, and M. Steinbacher, "Chapter 3 - dilatometry," in *Recent Advances, Techniques and Applications* (S. Vyazovkin, N. Koga, and C. Schick, eds.), vol. 6 of *Handbook of Thermal Analysis and Calorimetry*, pp. 103–129, Elsevier Science B.V., 2018.

[18] H. H.-T. Corporation, "Principle of Dynamic Mechanical Analysis (DMA) : Hitachi High-Tech Corporation."

[19] J. Li, T. Guan, Z. Zhang, Y.-T. Fu, F.-L. Guo, P. Huang, Z. Li, Y.-Q. Li, and S.-Y. Fu, "Orientation of discontinuous fillers in polymer composites: modelling, characterization, control and applications," *Progress in Materials Science*, vol. 148, p. 101360, 2 2025.

[20] B. Leszczynski, J. Skrzat, M. Kozerska, A. Wrobel, and J. Walocha, "Three dimensional visualisation and morphometry of bone samples studied in microcomputed tomography (micro-ct)," *Folia morphologica*, vol. 73, p. 422–428, 12 2014.

[21] K. Breuer and M. Stommel, "Rve modelling of short fiber reinforced thermoplastics with discrete fiber orientation and fiber length distribution," *SN Applied Sciences*, vol. 2, 1 2020.

[22] C. Geuzaine and J.-F. Remacle, "Gmsh: a three-dimensional finite element mesh generator with built-in pre- and post-processing facilities," *International Journal for Numerical Methods in Engineering*, vol. 79, no. 11, pp. 1309–1331, 2009.